2019-01-01

CFD Dem Analysis Of A Dry Powder Inhaler

Antara Badhan
University of Texas at El Paso

CFD DEM ANALYSIS OF A DRY POWDER INHALER

ANTARA BADHAN

Doctoral Program in Environmental Science & Engineering

APPROVED:

Vinod Kumar, Ph.D., Chair

V M Krushnarao Kotteda, Ph.D., Co-chair

Craig Tweedie, Ph.D.

Jose F. Espiritu, Ph.D.

Stephen L. Crites, Jr., Ph.D.
Dean of the Graduate School

Dedication

To My Daughter Aaveera , My Parents Md Abdur Rahman Mia, Nurzahan Begum & My Husband Mohammad Arif Ishtiaque Shuvo

CFD DEM ANALYSIS OF A DRY POWDER INHALER

by

ANTARA BADHAN, MS.C

DISSERTATION

Presented to the Faculty of the Graduate School of

The University of Texas at El Paso

in Partial Fulfillment

of the Requirements

for the Degree of

DOCTOR OF PHILOSOPHY

Environmental Science & Engineering

THE UNIVERSITY OF TEXAS AT EL PASO

December 2019

Acknowledgements

Thank you to my supervisor, Dr. Vinod Kumar for providing guidance and feedback throughout this project. A special thanks to Dr. Murali Kotteda for his guidance and help throughout whole time. I'm truly grateful to Dr. Craige Tweedie for believing me and guiding when required. My heartiest thanks to Ms. Lina Hamdan for her support and guidance throughout this journey. I would like to thank Department of Energy (DOE), National Energy Technology Lab (NETL) and Sandia National Labs for all of their support.

Abstract

Dry powder inhalers (DPIs), used as a means for pulmonary drug delivery, typically contains a combination of an Active Pharmaceutical Ingredient (API) and significantly larger carrier particles. The micro-sized drug particles - which have a strong propensity to aggregate and a poor aerosolization performance - are mixed with significantly large carrier particles that are unable to penetrate the mouth-throat region to deagglomerate and entrain the smaller API particles in the inhaled airflow. The performance of a DPI, therefore, depends on entrainment the carrier-API combination particles and the time and thoroughness of the deagglomeration of the individual API particles from the carrier particles. Since DPI particle transport is significantly affected by particle-particle interactions, very heterogeneous particles sizes and shapes, various forces including electrostatic and Van der Waals forces, they present significant challenges to Computational Fluid Dynamics (CFD) modelers to model regional lung deposition from a DPI. In the present work, we develop a novel high fidelity CFD Discrete Element Modeling (CFD-DEM) method and sensitivity analysis for predicting the transport and deposition for DPI carrier and API particles. The proposed development will leverage exascale capable CFD-DEM and sensitivity analysis capabilities from Department of Energy (DOE) laboratories: Multiphase Flow Interface Flow Exchange (MFiX) and DAKOTA UQ software, and Trilinos portable scalable linear algebra libraries. We validate the models with available data from the literature for DPI and conduct a sensitivity analysis of various formulation properties and their effects on particle size distribution with DAKOTA. Ideal particle size can be determined based on residence time for better DPI performances and respiratory deposition. Current analysis shows that drug particles of 1-3.66 μm show a higher drug dispersion and better aerosolization behavior with carrier particles between 51-63 μm on basis of residence time.

Table of Contents

List of Tables

List of Figures

Chapter 1: Introduction

1.1 Overview

Asthma is one of the most chronic distressing diseases in the United States. It is a rapidly escalating pulmonary disease that causes breathlessness, chest tightness, coughing and forced breathing [1]. Dry powder inhalers (DPI) directly deliver the drug to the target areas and provide more drug choices especially for those poorly absorbed orally [1–7]. These methods result in rapid onset of activity with small doses compared to injection and oral administration. In addition, DPIs do not contain chlorofluorocarbons (CFC). On the other hand, metered-dose inhalers contain CFC and damages the ozone layer. In general, drug particles of size less than 5 μm are used for the application in DPIs. In inhalation process, the particles are mixed with larger carrier particles as they are very cohesive and have poor flowability. The agglomerates disintegrate into small fractions or the drug particles detach from the carrier particle for the delivery of drugs to the lungs. Therefore, the cohesive/adhesive forces have to be sufficiently strong to aggregate and transport the particles, but weak enough to be overcome by the removal forces generated during the de-agglomeration process [8–10]. In addition, the adjustment of attachment between medicate particles and bond amongst bearer and medication particles was likewise found to influence the DPI performance [11, 12]. To better comprehend the systems of the agglomeration and deagglomeration forms, numerous examinations have been directed to investigate the impacts of particle shape [13], particle size [14–17], particle concentration [18], particle surface roughness [19], density and porosity [20], surface energy [21], material properties [22], storage conditions [23], crystal form [24], electrostatic charge [25], flowability [26] and the type of ternary additives [27] on the performance of dry powder inhalers. Those customary and progressed test approaches gave a point by point comprehension of the overseeing factors in DPIs. Notwithstanding, it is to a

great degree hard to recognize the impact of a solitary factor on DPI execution because of the many-sided quality of DPI systems [28]. The instruments of the agglomeration and deagglomeration forms are still inadequately comprehended [29].

Numerical simulations are widely in investigation of fluid flow and particle behavior. In Computational fluid dynamics (CFD), Navier-Stokes equations are discretized with a numerical method to simulate both laminar and turbulent flows [30–33]. Flow patterns as well as inhaler optimization are possible with CFD as well [34–36]**.** On the other hand, the discrete element methods (DEM) [37–39] provide detailed information of a particulate system at the single particle level. The particle trajectory is easy to obtain with this method unlike conventional experiments. It gives the connection between the macroscopic and microscopic properties of particulate matter, which is crucial in investigation of dry powder inhalers [40]. In addition, coupling DEM with CFD enables the approach to model the interactions between the fluid and particles [41**,** 42]. However, recent improvements to DEM can accommodate the electrification phenomenon [43] and the particles with irregular shapes [44].

1.2 OBJECTIVE

In the present work, numerical code Multiphase Flow with Interphase eXchanges (MFiX) is used for simulations. This software can model chemical reactions and heat transfer in dense and dilute gas–solid flows. Cartesian coordinate systems are used to solve the transport equations. The purpose of this present work is to show the range of validity for using simulations based on a 2D Cartesian coordinate system to assess a rectangular fluidized bed with different parameter. The simulations will be conducted for different inlet gas velocities with different particle diameter, which correspond to the bubbling and slugging regimes of fluidized beds. After these studies, we

will try to develop a novel high fidelity discrete element (CFD-DEM) method and sensitivity analysis is carried out for predicting the transport and deposition as well as the agglomeration and deagglomeration for DPI carrier and API particles. The CFD-DEM algorithm models agglomeration and deagglomeration forces with MFiX. We will validate the models with available data from the literature for DPI and conduct a sensitivity analysis of various formulation properties and their effects on particle size distribution with DAKOTA. Based on the available data from the literature for DPI, carrier and drug particle size has been chosen and MFiX-DEM analysis will be done on these ranges to obtain better DPI performances. The objective of this study is to obtain the DPI performance over large range of particle sizes on basis of particle residence time using MFiX-DEM method. As device performances also depends on the fluid flow inside inhaler domain, Computational Fluid Dynamics (CFD) analysis will be done to visualize the flow inside DPI.

1.3: PROJECT OUTLINE

This dissertation contains a total of 6 chapters:

- Chapter 1 gives a brief idea of the project and focus on the following chapters. This chapter discusses the use and benefits of dry powder inhaler and also explains the project objective.
- Chapter 2 in this thesis describes the past literature that contributes to the concepts used in this thesis. Different types of inhaler and a detailed background on DPI is discussed on that chapter.
- Chapter 3 focuses on the problem statement, specifically focused in building a framework that can solve the problem directly related to these applications.

- Chapter 3.2 schematically explains the framework of integrating MFiX-DAKOTA-Trilinos softwares in order scale the fluidized bed problem and for predicting the transport and deposition of DPI particles. This thesis discusses the development of an exascale capable framework that handles the computational fluid dynamics and uncertainty quantification methodologies involved for predicting the transport and deposition of DPI particles.
- Chapter 4 discusses the associated softwares like Multiphase Flow Interface Flow Exchange (MFiX) and DAKOTA UQ software, and Trilinos portable scalable linear algebra libraries used in developing the framework of Chapter 3. This chapter covers the motivation and detailed capabilities of these softwares and their implementation in computational modeling.
- Chapter 5 shows the results obtained from solving the fluidized bed problems with different parameters and different sizes of computational domain with DPI and analyzes the performance of DPIs on MFiX-DEM simulations.
- Chapter 6 summarizes the work completed and concludes the current thesis outcomes based on the results obtained on previous chapter. The scope for future work is also discussed for further improvements of this research possibilities.

Chapter 2: Background & Literature Review

2.1: Introduction:

The development of inhalation device is very important to deliver adequate quantity of inhaled drug to lungs. Oral inhalation drug delivery needs to aerosolize the drug compound in delivery device. To aerosolize drug compounds, three major approaches have been used; liquid drugs can be volatilized with compressed air or oxygen mixtures that consequently are breathed in, liquid solutions or solid powders can be pneumatically fluidized into a dispersed aerosol stream that is inhaled, or solid powders can be dispersed into a stream of passively inhaled air [44, 45]. The design of the device should have an environment where the drug can maintain its physicochemical stability and produce reproducible drug dosing [6]. Different types of inhaler devices are commercially used for asthma and chronic obstructive pulmonary diseases (COPD). In this chapter, we will discuss about different types of inhaler and previous studies on DPI that have dealt in problems of DPI and DPI particle transport over fluidized bed applications and how it is implementing in high performance computing.

2.2: Types of Inhaler:

For asthma and COPD medicines, different types of inhaler devices are used: metered-dose inhalers (MDIs), dry powder inhalers (DPIs) and mist inhalers. The most common and older form of inhalers are called metered dose inhalers (MDIs). The basic principle of MDI is by pressing down on the inhaler top, which release a liquid amount of the medicine into the lungs, when inhalation occurs at the same time. These devices are made of three standard components- a metal canister, plastic actuator, and a metering valve. In MDIs, medication or capsule is usually stored in solution in a pressurized canister which contains a propellant [46]. The propellants should be

nontoxic, nonflammable, and compatible with drugs formulated either as solutions or suspensions [47]. The metal canister is attached to a plastic, hand-operated actuator. This type of inhaler discharges a fixed dose of medication in aerosol form while activated. The exact method of using an MDI is to first fully exhale then place the mouth-piece of the device into the mouth, and afterward inhale at a moderate rate which depends on patient's condition and dosage, and at last press down the canister to release the medicine. Some inhalers are made in such a way that may act later and others are made to act instantly in case of an asthma attack. The schematic of a metered dose inhaler (MDI) are shown in Figure 2.1.

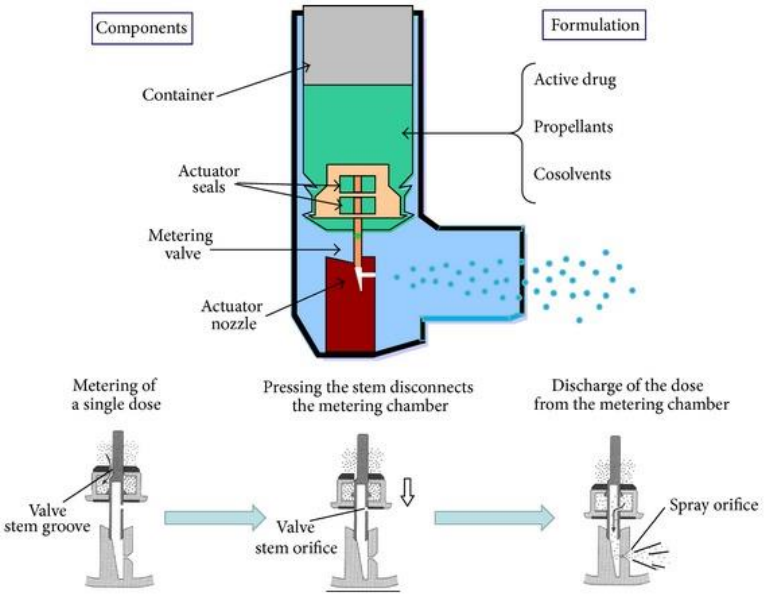

Figure 2.1: Schematic and working principle of metered dose inhalers (MDIs) [5]

Due to the change of asthma inhalers profile and needs, there is another type of inhalers where propellant is being used in the form of a dry powder is called dry powder inhaler or DPI. Like a metered dose inhaler, DPI is a handheld device that delivers a measured dose of asthma medicine accurately in the form of dry powder into the lungs. The DPIs design has been advanced in such a way that the device should generate adequate turbulence and particle–particle collisions to separate the drug particles from carrier surface of an interactive mixtures or deagglomerate

particles from large agglomerates of drugs only [48]. To prepare the dose for fluidization with tangential flow of air at the time of patient inspiration, most of the DPI devices are primed by pressing (Rotahaler®), sliding (Spinhaler®), rotating (Twisthaler®) or piercing (Handihaler®) [49]. Then the fluidized powder is passed through a screen to deagglomerate particles for deep lung delivery. The main difference between a DPI and a MDI is that in DPI, powder is kept in small amounts in different chambers instead of "press/squirt/inhale" action like MDI. In a DPI, the medication comes in a dry powder form. A small capsule, disk, or compartment inside the inhaler device is used to hold the medication [50, 51]. The schematic of a dry powder inhaler (DPI) is shown in Figure 2.2.

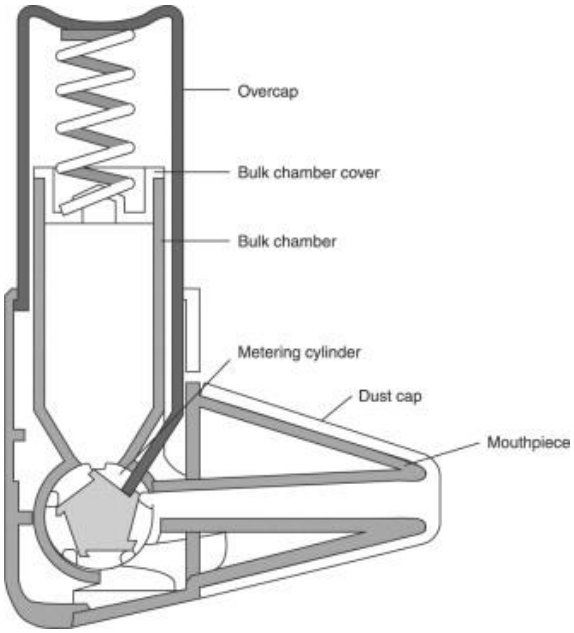

Figure 2.2: Schematic of dry powder inhaler (DPI) [9]

This device consists of a metering system, an actuator and the dry formulation. The bulk chamber is covered by an over-cap and holds the formulation. A dust-cap is used to cover the mouth-piece for preventing contamination. The metering valve extracts the powder from the chamber and moves it forward to the mouth-piece for inhalation. A dry powder inhaler (DPI) delivers the drug in the form of particles confined in a capsule or blister which needs to be

punctured before use. The patient requires a negative inhalation to deliver the medication as 'respirable' aerosol [52]. The working principle of a DPI is pretty simple, which is discussed below:

- A strong inhalation may require several seconds.

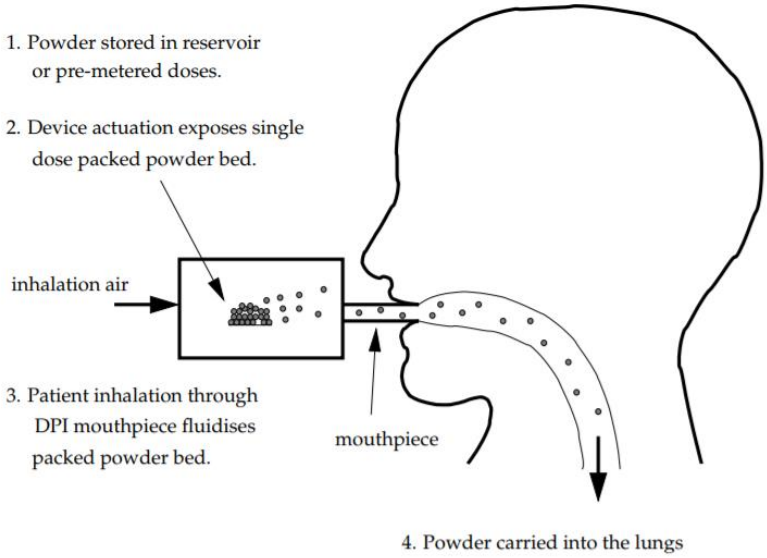

Figure 2.3: DPI operation from actuation to lung delivery[51]

- Patient will have to place the inhaler's mouthpiece in his mouth and close his lips tightly around the mouthpiece.
- After rotating the inhaler chamber or clicking a piece on the inhaler, patient is required to inhale quickly and deeply through his mouth for few seconds which releases the medicine directly to the lungs.
- After the medicine is inhaled, breath should be held for a few more seconds to let the medicine settle in lungs. Then the patient can breathe out slowly through pursed lips.

- It is recommended to hold the inhaler away from mouth while you breathe out. It can blow the powder medicine out of the inhaler and the moisture from breath can cause the dry powder to clump together and clog the inhaler.
- As this type of inhaler does not contain a propellant, so it needs a sufficient inspiratory flow rate for drug delivery. Because of this requirement of an inspiratory flow, this type of devices (DPIs) are not suitable for the treatment of acute asthma attacks [53].

2.3: DPI BACKGROUND:

The pressurized metered-dose inhaler (pMDI) was invented by Irvine Porush and George Maison in 1955 and became the most commonly used device to deliver inhaled asthma drugs on that time. Pulmonary drug delivery via pMDIs, DPIs or nebulizers are the preferred treatment methods for asthma patients. The pressurized metered-dose inhalers (pMDIs) were the most commonly used inhaler devices for asthma and COPD patients for many years. But after implementing the Montreal Protocol in 1987 for limited use of CFCs in MDIs, DPIs became the most preferable devices [54]. To overcome the problems associated with nebulizers and MDIs, dry powder inhalers were developed to provide an alternative way of delivering medication to the lungs. With the advancement of science and technology, pulmonary delivery of drugs has become the route of choice after the introduction of the DPI in 1967. After the development in 1960s and 1970s, the original DPI devices used patient's inspiratory flow to disperse the aerosol from capsule unit doses and deliver it to the airways [55].

There are a significant number of commercial dry powder inhalers available, which vary in dispersion efficiency because of their design characteristics. There has been lots of development

done on DPIs after that. There are lots of commercially available DPI devices exist in market based on their dosage capability, breathe activated and power driven properties. Based on the design, DPI devices are categorized into three wide groups, i.e., the first generation DPIs, the second generation DPIs and the third generation DPIs [52]. The first-generation DPIs were small, breath activated single unit capsule-based passive devices like Spinhaler® and Rotahaler®. With better technology, the second-generation DPIs depend on more sophisticated devices, such as reservoirs and micronized powders (e.g., Turbohaler) [56]. The third and newer generation DPIs are active, power-assisted inexpensive devices that are highly dispersible and can incorporate with battery-driven impellers and vibrating piezo-electric crystals (e. g. MicroDose ® ; MicroDose Therapeutx, Monmouth Junction, N.J., USA) [57].

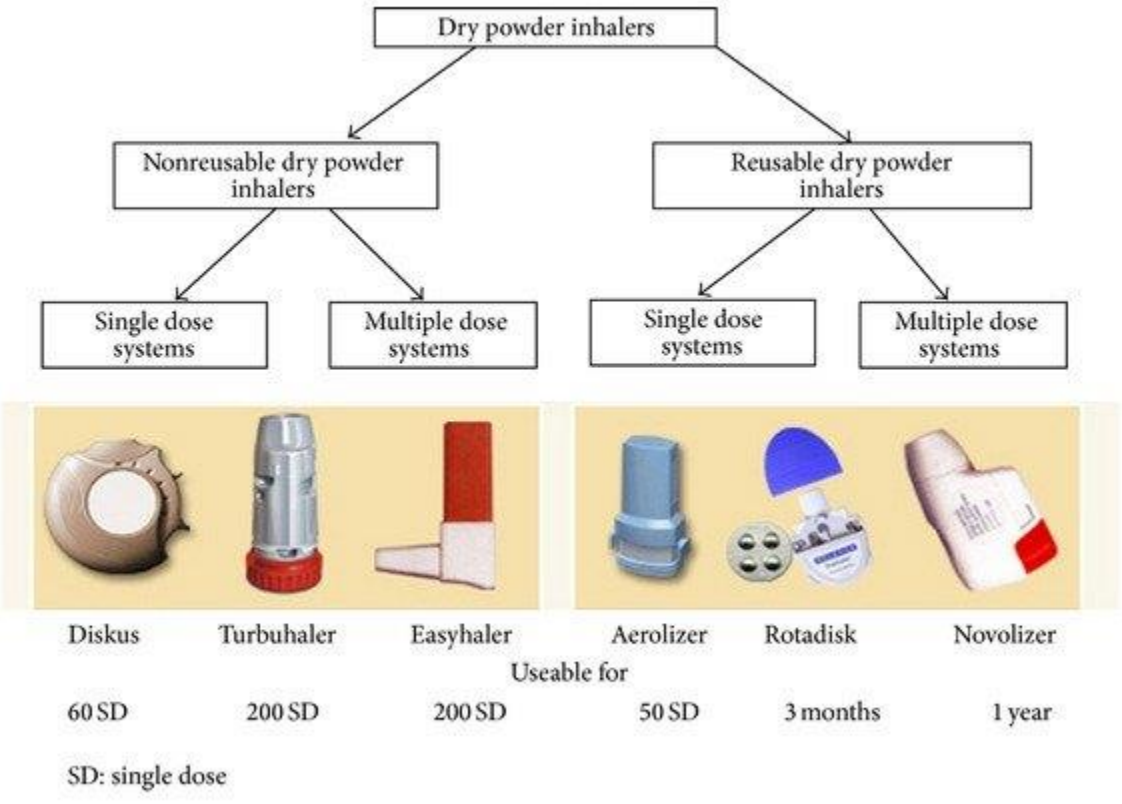

Figure 2.4: Different types of dry powder inhalers (DPIs) [51]

Numerous studies have been done on successful delivery of drugs into the deep lungs which mainly depends on the amalgamation between powder formulations and the device performance [58]. Voss and Finlay developed a powder de-agglomeration device to investigate the effects of turbulence and mechanical impact on dry powder de-aggregation which showed that the range of de-aggregation increased as the level of turbulence was increased [59]. In order to explore in which rate API particles are detached from carrier particles in an air classifier, a study found that the rate increased with increasing flow rate and dispersion time [60]. Another research showed an aerodynamic dispersion of loose aggregates in a uniform fluid flow using DEM–CFD and found a threshold velocity above which dispersion occurred rapidly and approximated equilibrium asymptotically [61]. All of these works showed the overall DPIs behavior and the mechanical analysis of dispersion behavior of loose agglomerate. Lots of studies have been done on the particle size of inhalation aerosols. Many studies showed that the optimal aerodynamic diameter for DPIs are between 1 and 5 mm when they are operated at inspiratory peak flow rates between 30 and 150 L/min [62]. The wider size distribution in DPIs may benefit the distribution throughout the lungs. However, other researches indicated that use of monodisperse particles or narrow size distributions with controlled inspiratory flow rates and inhaled volumes, shows better aiming of particular deposition sites, as well as reducing adverse side effects [60].

2.4: SUMMARY:

The inhalation of asthma medicine in powder form may reach instantly the lungs without producing any type of coughing. The use of very fine powdered medicine in miniscule doses can be very effective in DPI. Though DPI is much more advanced than MDI, it has also some limitations. DPI may not be suitable for very young children and people with extremely weak

breath. Since DPI particle transport is significantly affected by particle-particle interactions, very heterogeneous particles sizes and shapes, various forces including electrostatic and Van der Waals forces, they present significant challenges to CFD modelers to model regional lung deposition from a DPI. Though lots of investigations have been done in DPI and DPI particle transport, but carrier-based DPIs at the micro-mechanical level investigation was hardly reported.

Chapter 3: Problem Definition

3.1: INTRODUCTION:

This thesis discusses the development of an exascale capable framework that handles the computational fluid dynamics and uncertainty quantification methodologies involved for predicting the transport and deposition of DPI particles. For handling such a large scale scientific applications via enhanced communication, robust memory management and integration of the CFD and UQ interface, the framework is required. The objective of this project is to show the range of validity for using simulations based on a 2D Cartesian coordinate system to assess a rectangular fluidized bed with different parameter. And the next step will be to develop a novel high fidelity discrete element (CFD-DEM) method and sensitivity analysis for predicting the transport and deposition as well as the agglomeration and deagglomeration for DPI particles. This chapter focuses on the problem statement, specifically addressed in building a framework that can solve the problem directly related to these applications.

3.2: PROBLEM DEFINITION:

Figure 3.1 illustrates the schematic of a framework that integrating the CFD and DEM interface. This project will integrate the CFD and DEM interface for commercially available inhaler device. The framework employs NETL developed CFD-DEM simulation code “MFiX” for predicting the transport and deposition of DPI particle, ANSYS.INC developed engineering simulation and 3D design software ANSYS for visualizing the fluid flow and particle movement and Sandia developed “DAKOTA” for sensitivity analysis. There are lots of drug and carrier particle information available in previous researches. This project is mainly focus on the particle properties in DPI performances. After doing all parametric studies, cases has been setup for all

particle and fluids data variation for this project. Simulations will be done by using two CFD-DEM simulation Codes such as MFiX & ANSYS. Input files needs to be created for MFiX simulations by developing codes in C++. This code generates values of input variables and passes those input variables to MFiX-DEM and launches MFiX simulations. After numerical calculations, ParaView performs post-processing to extract the quantities of interest from MFiX–DEM results. After obtaining all the data from MFiX and ParaView, particle data analysis will be done.

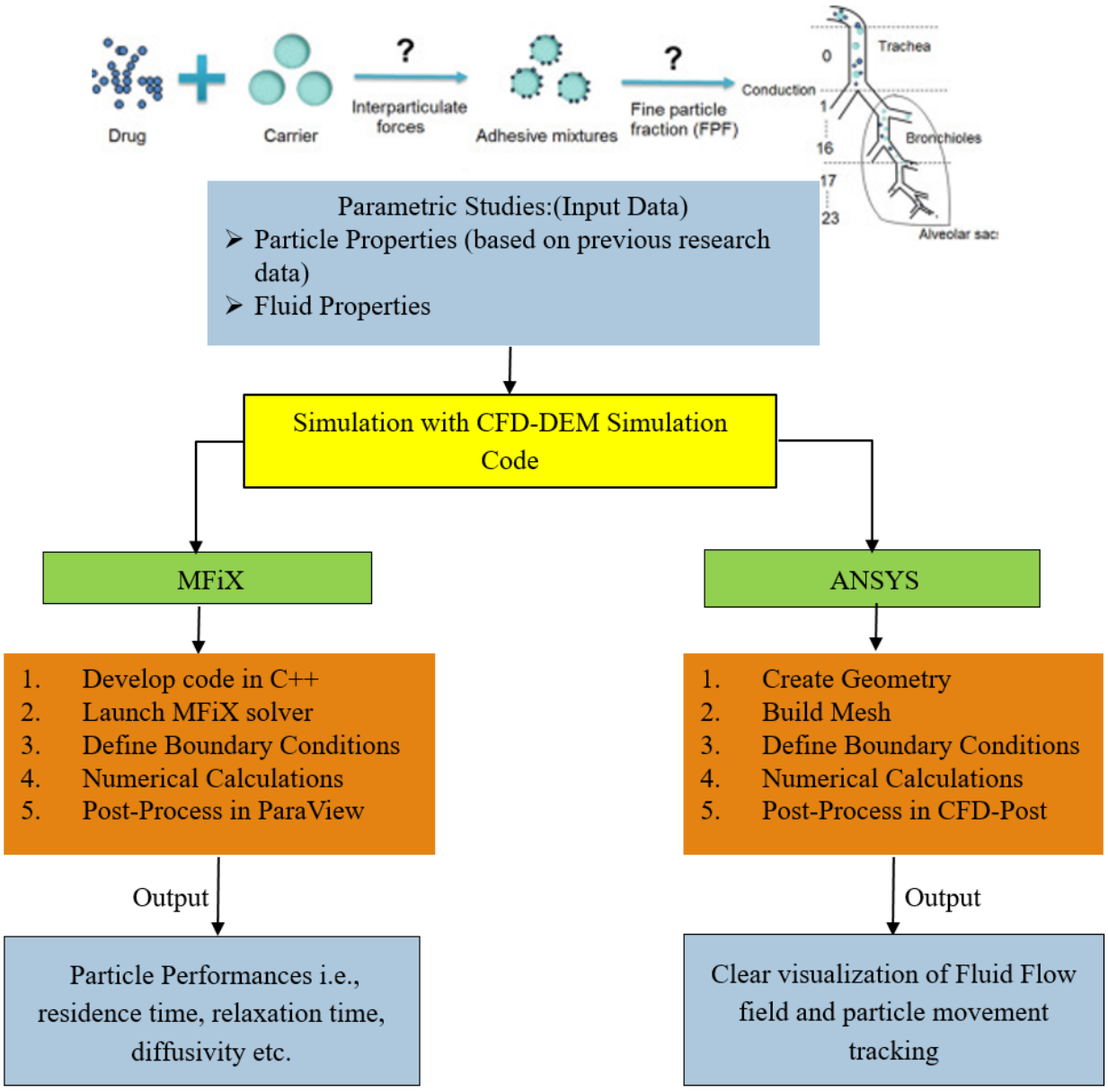

Figure 3.1: Project Schematic and simulation procedure based on the CFD-DEM method

Another simulation will be done using CFD-DEM simulation Code ANSYS which best describes the flow field and particle tracking inside a computational domain. From geometry creation to post-processing all can be done in this one software package. Same geometric parameter and fluid and particle properties will be used in this software. After geometry and mesh creation, input variables will be implemented in ANSYS FLUENT to run the case. When calculations will be done then post-processing can be done in CFD-Post to get better idea of flow field and particle movement inside the domain.

For the uncertainty quantification an interface between the MFiX and DAKOTA is created via a C++ wrapper of MFiX-DEM simulations. This wrapper exchanges the information among DAKOTA and MFiX–DEM for the uncertainty quantification. DAKOTA generates values of uncertain input variables via upper and lower bounds and passes those input variables to MFiX-DEM via the wrapper and launches MFiX simulations. DAKOTA receives response functions from MFiX and performs the uncertainty quantification. Then performs post-processing to extract the quantities of interest from MFiX–DEM results. In the input file for DAKOTA, the variables with uncertainty and a range of values are used to determine the upper and lower bounds.

Present study deals with a dry particle inhaler (DPI) which is considered as a fluidized bed for simulation eases. The schematic of a DPI computational domain and boundary conditions used in this research is shown in Figure 3.2. The DPI device is considered as a fluidized bed where the different types of particles will react, agglomerates and then leave the domain after a certain time. Figure 3.2 shows the computational domain and boundary conditions for the DPI problem.

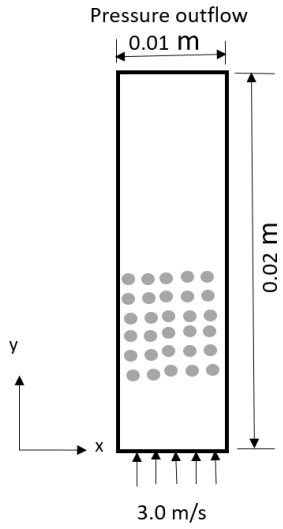

Figure 3.2: Computational domain and boundary conditions for the DPI problem.

The geometrical dimensions of fluidized bed with other conditions used in this study are given in Table 3.1.The parameters used in Table 3.1 will be same for MFiX and ANYS simulations.

Table 3.1: Particle properties with Geometric configuration of fluidized bed used for this project

Parameters	**Value/Conditions**
Bed length	0.02m
Bed width	0.01m
Solver	Pressure-based
Inlet Condition	Velocity Inlet
Outlet Condition	pressure outlet
Wall	No-slip
Discrete Element Method	On
Inlet DPM case	Escape
Outlet DPM case	Escape
Wall DPM case	Reflect
Spatial Discretization	First Order Upwind
Particle stiffness coefficient	1000 N/m
Particle friction coefficient	0.1 m
Fluid Velocity	1-5 m/s
Temperature	293.15 k
Gravity (in y direction)	-9.81 m/s
Gas Viscosity	1.81E-05 kg/m.s
Number of Particles	500 drug particle 500 carrier particle

Several cases with change of fluid and particle properties (size, density) will be simulated to analyze particle characteristics and their performances on lung deposition. All the cases will be simulated in MFiX 18.1.0 software and the data from MFiX will be post-process via ParaView 5.6.0. More than 30 cases have been running yet and from data analysis of those cases, few cases will be chosen that show better results with particle variations in this project. All of the cases are shown in Table 3.2.

Table 3.2: Particle properties used in this research

Case	Drug Particle Diameter, μm	Carrier Particle Diameter, μm
1	3.11	56
2	4.50	63
3	3.26	63
4	3.33	63
5	3.30	63
6	3.30	63
7	3.10	69
8	2.90	63
9	2.90	63
10	1.80	72
11	2.63	59
12	1.80	71
13	1.80	52
14	3.80	48
15	2.40	51
16	3.40	50
17	3.10	53
18	3.10	5.1
19	3.45	41
20	3.50	54
21	3.50	61
21	3.40	43
22	2.56	53
23	2.50	59
24	3.15	56.9
25	1.80	41
26	4.51	71
27	1.92	51.3
28	5.14	63.7

29	3.04	42
30	3.66	47.3
31	1.74	64.2

Based on a wide range of particle data, overall particle performances will be measured as a parameter of particle relaxation time, residence time, and diffusivity. Change of particle size will directly impact the tangential and axial velocity components and all other particle properties. In this research, a 2D full order high-fidelity CFD tool will be used to simulate the fluid and particle flow inside a DPI device to evaluate different particle size options for optimizing particles performances in terms of relaxation time, residence time, and diffusivity. After comparing all the results, it will be simple to predict the best case scenario.

3.2.1: Modeling using MFiX:

We considered a fluidized bed in two dimensions in figure 3.3 shows for the DPI problem created in MFiX. The length, width of the bed are 0.02 m and 0.01 m, respectively.

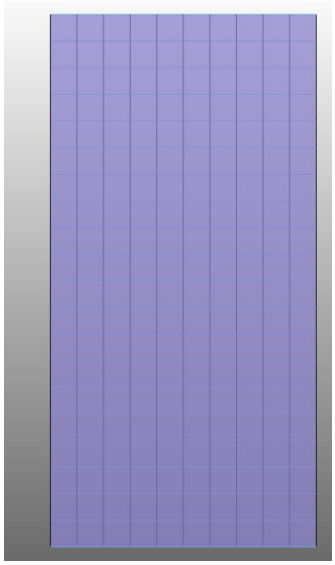

Figure 3.3: Computational domain for the DPI problem on MFiX. The figure is drawn to scale.

The computational domain is discretized with 20 equi-spaced cells in the axial direction (y-direction) and 10 equi-spaced cells in the normal direction (x-direction). Velocity along the x-

direction is specified on the bottom boundary. The pressure outflow condition is applied on the top boundary. Initially, the bed is filled with 500 carrier particles of 52.5 μm in size and density of 2650 kg/m^3 and 500 drug particles of 3.2 μm in size and density of 1520 kg/m^3. These particles are fluidized with air of velocity 3 m/s, density 1205 kg/m^3, and viscosity of 18 $\mu P.s$. Gravity is considered. The stiffness coefficient of the particle is 1000 N/m. The friction coefficients of particles is 0.1.

A 3D fluidized bed is also created and the data from 3D cases will be used in DAKOTA to perform the uncertainty quantification. Then post-processes the data to extract the quantities of interest from MFiX–DEM results. The length, width and height of the bed are 0.01 m, 0.01m and 0.02 m respectively.

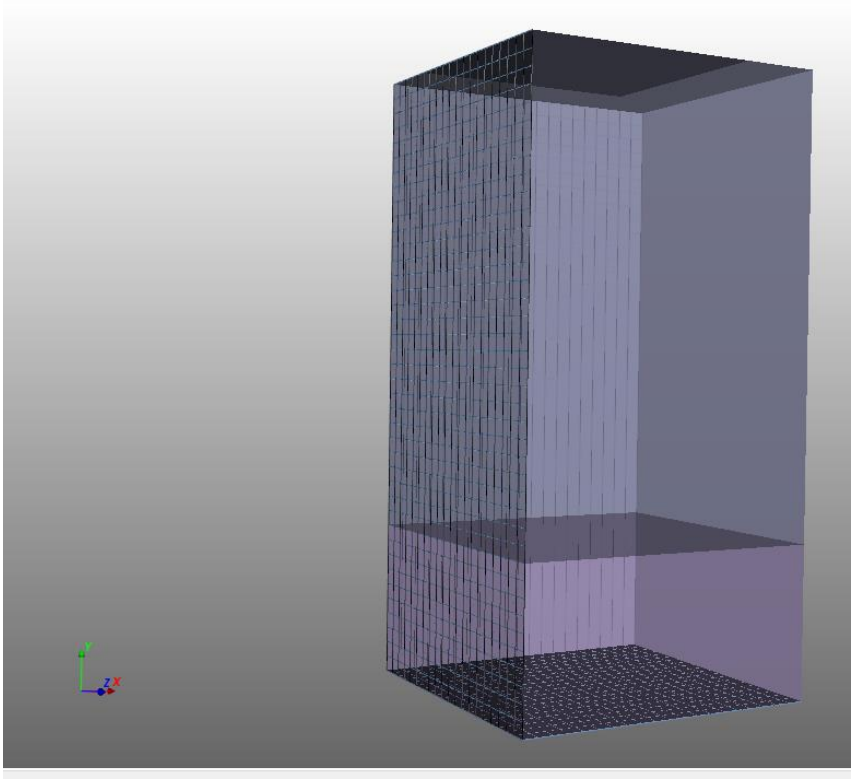

Figure 3.4: Computational 3D domain for the DPI problem on MFiX. The figure is drawn to scale.

This 3D computational model will deal with approximately 8000 particles inside the domain, so MFiX-PIC (particle in cell) solver is used in this case. For 2D cases, MFIX-DEM (Discrete Element Method) is used because of it good fidelity and ability to model individual particles of the solid phase. But for dealing with a large amount of particle, it is not user-friendly and will require high performance computing (HPC) resources and lots of time. For this reason, 3D simulations for larger amount of particle use PIC model instead of DEM on MFiX.

Velocity along the x-direction is specified on the bottom boundary. The pressure outflow condition is applied on the top boundary. The outlet is located on middle of the top boundary where outlet dimension is 0.005*0.005 m. Same size of particles are used in both 2D and 3D cases.

3.2.2: Modeling using ANSYS:

The same fluidized bed with same dimension is considered but with different software which is shown in Figure 3.5. ANSYS is used to visualize the fluid flow inside the domain. The length, width of the bed are 0.01 m and 0.02 m respectively. The computational domain is created with ANSYS Workbench and meshing has been done using ANSYS MESHING. Cells are discretized with Global Coordinate Method. All quadrilateral type of mesh is created with Mapped facing option that will ensure smooth flow into the domain. Total 222111 elements with 223112 nodes have been created for fine meshing. Velocity along the x-direction is specified on the bottom boundary. The pressure outflow condition is applied on the top boundary. The mesh operation was done at the end to make the geometry prepared for numerical fluid flow analysis within the area. When the geometry has a finer mesh with no skewed elements then fluid flow inside an inhaler device can be solved in ANSUS FLUENT 15.0. A commercially available CFD code,

FLUENT is used to solve the discretized equations (conservation of mass, momentum and energy equations) by finite volume formulation.

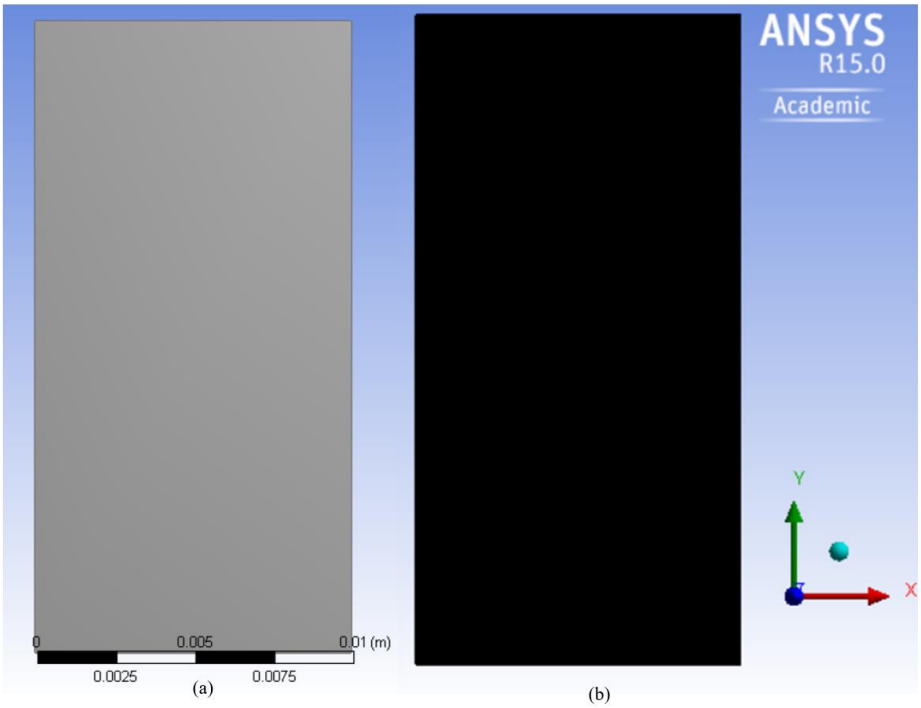

Figure 3.5: (a) Computational domain and (b) mesh generation for the DPI problem. The figure is drawn to scale.

Once the modeling had done, boundary condition was implemented. In this study, a velocity inlet boundary condition is applied at inlet; pressure outlet BC at outlet and no slip BC at the walls. Air was considered as continuous phase material in this study. The Eulerian-Lagrangian approach has been employed to simulate the DPI device. Numerical simulations were done by the Eulerian reference frame for continuous gas phase flow and by Lagrangian method for dispersed phase particle trajectories. 3-D, unsteady and incompressible fluid flow in Eulerian formulation is introduced in this investigation. The Lagrangian approach resolves the transport equations of continuous phase in Eulerian frame and then integrates the dispersed phase equations by tracking individual spherical particles through the converged flow field. The stochastic Particle Tracking Model outlined the particle motions by tracking particle trajectories in Lagrangian frame of reference. By keeping track on the number of particles escaping through the outflow, the

particle performance could be measured. There are a lot of turbulence model available in FLUENT solver. As other models (i.e.-ε, k-omega) models have some limitations to swirling turbulent flow, so for simple flow field, laminar model is used in this simulation. The fluctuating gas velocities can be determined by using a discrete random walk (DRW) model which is based on the stochastic tracking scheme.

The Phase coupled SIMPLE (Semi-Implicit Method for Pressure-Linked Equations) scheme for pressure – velocity coupling has been used in finite volume method to discretize the partial differential equations and second order upwind scheme is used in the solution method for the control volume variables. The inlet velocity is considered as 3 m/s for this study .The maximum number of integration steps were 5×10^5 and a length scale of 0.005m were chosen for the dispersed particle trajectories. Particle time step size of 0.001s with an automated tracking scheme was selected for the numerical experiments and an accuracy of 10^{-5} was performed for accuracy control.

3.4: Summary:

This chapter provides a high level description of the objective of this research. It discusses about the framework that employs NETL developed CFD-DEM simulation code "MFiX" for predicting the transport and deposition of DPI particles and Sandia develop "DAKOTA" for sensitivity analysis. This chapter also discusses about a 2D fluidized bed domain and its different boundary conditions for MFiX and ANSYS simulation. There will be different cases with the change of boundary conditions such as, change in particle size, density and also change in fluid properties.

Chapter 4: Methodology

4.1: Introduction:

Several commercial packages are available for analyzing computational modeling problems associated with fluid dynamics applications. Despite the advancement of computational modeling packages, there are lots of challenges in resolving physics in a large computational domain with plenty resolutions. This research will influence exascale capable CFD-DEM and sensitivity analysis capabilities from Department of Energy (DOE) laboratories: Multiphase Flow Interface Flow Exchange (MFiX) and DAKOTA UQ software, and Trilinos portable scalable linear algebra libraries. In this chapter, we will discuss details about these softwares and their implementation in computational modeling. One of the software used in this study is MFiX that has generally been a popular CFD library to solve fluidized bed problems. Even though MFiX has been developed on a parallel FORTRAN platform, it has limitations with scalability issues for large and non-linear problems. In that regard, DAKOTA provides flexible and extensible problem-solving capabilities on high-performance computer and creates a flexible interface between simulation codes and analysis methods. Moreover, Trilinos has been explored for its scalability performance on dealing with linear algebra objects and state-of-the-art linear solver capabilities. The Trilinos library is integrated with MFiX in order to exploit the scalable linear algebra package in MFiX.

4.2 MFiX

MFiX is a widely used by the fossil fuel reactor communities to model and understand the multiphase physics in a circulating fluidized bed. In MFiX, the interactions between gas-solids are addressed by the solving the coupled continuity and momentum conservation equations simultaneously. The momentum conservation equations involve interaction force, or momentum transfer, between the gas phase and the various solids phase. From studies on the dynamics of a particle, several mechanisms, such as electrostatic forces, van der Waals force, drag force,

buoyancy, virtual mass effect, lift force, Magnus force, Basset force, Faxen force, and forces caused by temperature and density gradients, play important role in modeling multiphase flows. Several other factors, however, need to be considered when the formulas for a single particle system are generalized to describe interaction forces in real life multi-particle systems such as: 1) the effect of the proximity of other particles must be accounted for; the single-particle interaction force must be corrected to account for the effect of mass transfer between the phases, as in the case of coal devolatilization or combustion, for example; 2) the momentum transfer accompanying such mass transfer must be included in the interaction force; and 3) the formulations for fluid-solids drag deal with uniform, smooth, spherical particles, whereas practical fluid-solids systems contain rough, non-spherical particles of different sizes [63]. The particle-size distribution can be characterized by an average size based on particle surface area. A broad particle-size distribution can be discretized into two or more particle surface area, each characterized by an average size. The effect of non-sphericity and roughness effects on drag are implicitly contained in the momentum conservation equations, but it may be appropriate to explicitly account for the particle interactions on the fluid-solids interaction force for non-spherical particles through a new drag model. Fluid-particle and particle-particle forces can be separated in two terms. Averaging the particle to granularize the system makes the hydrodynamic solver incapable of resolving small scale phenomena such wake-dominated features near the particles. In fossil energy applications, for example, gaseous molecules are produced and participate in radiant heat transfer as a result of thermal radiation with vibrational and rotational modes of energy absorption. The solid particles during this process also plays a major role in radiative heat transfer since the coal particles will go through preheating, devolatization, ignition and partial combustion process.

The state of art of multiphase flow is relatively new and not well understood. In DPIs, for example, APIs and carrier particles flows in a dense gas-solids mixture. The coupled physics include hydrodynamics, shear forces, and reaction kinetics. The coupled physics would clearly influence the performance of DPIs. Design of operational DPIs has traditionally relied on lab-scale experiments as pilot-scale units and clinical trials that are expensive to build and operate and provide limited insight.

In DEM approach, the gas-phase governing equations for mass and momentum conservation are like those in traditional gas-phase CFD but with additional coupling terms due to drag from the solids phase. The solids-phase is modeled using discrete particles. The governing equations [64,65] for the gas-phase continuity and momentum conservation in the absence of phase change, chemical reactions, growth, aggregation, and breakage phenomena, are:

$$\frac{\partial(\varepsilon_g \rho_g)}{\partial t} + \nabla.\left(\varepsilon_g \rho_g v_g\right) = 0, \tag{4.1}$$

$$\frac{D}{Dt}(\varepsilon_g \rho_g v_g) = \nabla.\overline{\overline{S_g}} + \varepsilon_g \rho_g\, g - \sum_{m=1}^{M} I_{gm}, \tag{4.2}$$

where, subscript *g* represents a fluid variable, subscript *s* represents the quantity belongs to the solid phase, ε is the volume fraction, ρ is the thermodynamic density, v is the volume-averaged gas-phase velocity, I_{gm} accounts the momentum between the fluid phase and the mth solid phase, buoyancy, and drag force, among others, and $\overline{\overline{S_g}}$ is the stress tensor. The stress tensor is given by $\overline{\overline{S_g}} = -P_g\,\bar{I} + \overline{\overline{\tau_g}}$, where P is the pressure and, $\overline{\overline{\tau_g}}$ is the stress tensor. The stress tensor is defined as $\overline{\overline{\tau_g}} = 2\,\mu_g\,\overline{\overline{D_g}} + \lambda_g\,\nabla.\mathrm{tr}(\overline{\overline{D_g}})\,\mathrm{I}$, where $\left(\overline{\overline{D_g}}\right) = \frac{1}{2}\left[\nabla v_g + \left(\nabla v_g\right)^T\right]$ is the strain rate tensor and μ_g and λ_g are the dynamic and second coefficients of viscosity. Conservation of species, internal energy, granular energy as well as correlations that model the flow at all ranges of Reynolds numbers can be found in [66–68].

In DEM approach, the m^{th} soild-phase is represented by N_m spherical particles with each having diameter D and density ρ. Solid phases are differentiated based according to radii and densities. The diameter and density of the m^{th} solid-phase is denoted by D_m and ρ_{sm}, respectively. For total of M solid phases, the total number of particles is equal to $N = \sum_{m=1}^{M} N_m$. These N particles are represented in the Lagrangian frame of reference at time t by $\{X^{(i)}(t), V^{(i)}(t), \omega^{(i)}(t), D^{(i)}(t), \rho^{(i)}, i=1,\ldots,N\}$, where $X^{(i)}$ denotes the i^{th} particle's position, and $V^{(i)}$ and $\omega^{(i)}$ represents its linear and angular velocities. The mass $m^{(i)}$ and moment of inertia $I^{(i)}$ of the i^{th} particle are equal to $\rho^{(i)} mD(i)^3 /6$ and $mD(i)^2 /10$, respectively. The position, linear and angular velocities of the i^{th} particle are calculated according to Newton's laws

$$\frac{dX^{(i)}}{dt} == V^{(i)}(t) \tag{4.3}$$

$$m^{(i)} \frac{dV^{(i)}(t)}{dt} = F_T^{(i)} = m^{(i)} g + F_d^{(i\in k,m)}(t) + F_c(t) \tag{4.4}$$

$$I^{(i)} \frac{d\omega^{(i)}(t)}{dt} = T^{(i)} \tag{4.5}$$

where, g is the acceleration due to gravity, $F_d^{(i\in k,m)}(t)$ is the drag force due to pressure and viscosity on i^{th} particle residing in k^{th} cell and belonging to the m^{th} solid-phase, $F_c^{(i)}$ is the net contact force acting because of contact with other particles, $T^{(i)}$ is the sum of all torques acting on the i^{th} particle, and $F_T^{(i)}$ is the net sum of all forces acting on the i^{th} particle.

To resolve the particle–particle and particle–wall collisions, a soft-spring model [69] is used. The details of the soft-spring mode implementation along with other numerical and implementation details can be found in the MFIX–DEM documentation [70]. Since a spring–dashpot combination is used in soft-spring model, it leads to introduction of several numerical

parameters (such as, spring stiffness coefficient, damping coefficient, etc.) that are related to physical parameters such as coefficient of restitution, coefficient of friction, etc.

For simulating multi-phase flow, MFiX has three numerical models: Two-Fluid Model (TFM), Discrete Element Model (DEM) and the Particle in Cell Model (PIC). TEM and PIC both are Eulerian-Eulerian model while DEM is an Eulerian-Lagrangian model, where instead of using the finite-volume-method, the second phase (typically solid particles) are treated as particles. The governing equations for such flows are given by the phasic volume fractions of each phase are as follows,

$$\epsilon_g + \sum_{m=1}^{M} \epsilon_{sm} = 1 \tag{4.6}$$

Here, g, s and m denote the gas phase, the solid phase and the m^{th} solid phase in the mixture of fluids. The effective densities of the gas and solid phases are given as

$$\rho'_g = \epsilon_g \rho_g \tag{4.7}$$

$$\rho'_{sm} = \epsilon_{sm} \rho_{sm} \tag{4.8}$$

Here, ρ'_g and ρ'_{sm} are effective densities while ρ_g and ρ_{sm} are their actual densities.

The continuity equations for the gas and the solid phase m are given as

$$\frac{\partial}{\partial t}\left(\epsilon_g \rho_g\right) + \boldsymbol{\nabla}.\left(\epsilon_g \rho_g \boldsymbol{v_g}\right) = \sum_{n=1}^{N} R_{gn} \tag{4.9}$$

$$\frac{\partial}{\partial t}\left(\epsilon_{sm} \rho_{sm}\right) + \boldsymbol{\nabla}.\left(\epsilon_{sm} \rho_{sm} \boldsymbol{v_{sm}}\right) = \sum_{n=1}^{N} R_{smn} \tag{4.10}$$

The first and second terms on the left sides of the equations are the rate of mass generation per unit volume and the net rate of convective mass flux. The terms of R_{gn} and R_{smn} on the right sides account for interphase mass transfer due to chemical reactions or physical processes.

The momentum equations are given as

$$\frac{\partial}{\partial t}(\epsilon_g \rho_g \boldsymbol{v_g}) + \boldsymbol{\nabla}.(\epsilon_g \rho_g \boldsymbol{v_g}.\boldsymbol{v_g}) = \boldsymbol{\nabla}.(S_g) + \epsilon_g \rho_g g - \sum_{m=1}^{M} I_{gm} + \boldsymbol{f_g} \quad (4.11)$$

$$\frac{\partial}{\partial t}(\epsilon_{sm} \rho_{sm} \boldsymbol{v_{sm}}) + \boldsymbol{\nabla}.(\epsilon_{sm} \rho_{sm} \boldsymbol{v_{sm}}.\boldsymbol{v_{sm}}) = \boldsymbol{\nabla}.(S_{sm}) + \epsilon_{sm} \rho_{sm} g - \sum_{l=1, l \neq m}^{M} I_{ml} + I_{gm} + \boldsymbol{f_g} \quad (4.12)$$

The first terms on the left sides of equations are the net rate of momentum generation and the second terms are the net rate of momentum transfer by convection. These include the gas phase and solid phase stress tensors S_g and S_{sm}, the body forces due to gravity g, the flow resistance force f_g due to internal porous surfaces, the interaction force I_{gm} accounting for the momentum transfer between the gas phase and the mth solid phase, and the interaction force I_{lm} between the m^{th} and l^{th} solid phases.

4.3 DAKOTA

UQ strategies are sorted by their capacity to spread aleatory or epistemic information vulnerability portrayals, where aleatory vulnerabilities are final changeability inalienable in nature and epistemic vulnerabilities are reducible vulnerabilities coming about because of an absence of information. Since adequate information is by and large accessible for aleatory vulnerabilities, probabilistic strategies are generally utilized for processing reaction appropriation measurements considering information likelihood conveyance. Then again, for epistemic vulnerabilities, any utilization of likelihood conveyances depends on subjective information instead of target information, and we may on the other hand investigate nonprobabilistic strategies considering interim. The aleatory UQ techniques in DAKOTA incorporate different testing-based methodologies (e.g., Monte Carlo and Latin Hypercube inspecting), neighborhood and global unwavering quality strategies, and stochastic extension (polynomial mayhem developments and stochastic collocation) approaches. The epistemic UQ techniques incorporate nearby and global interim investigation and Dempster-Shafer confirm hypothesis.

DAKOTA [71] is a toolkit that provides a flexible and extensible interface between simulation codes and analysis methods. It contains algorithms for optimization; uncertainty quantification with sampling, reliability, and stochastic expansion methods; parameter estimation with nonlinear least squares methods; and sensitivity analysis with design of experiments and parameter study methods. These capabilities are used in various optimization models. The toolkit provides flexible and extensible problem-solving capabilities on high-performance computers as the main components for the iterative system analyses are designed with an object-oriented framework. In the present work, DAKOTA will used to perform the uncertainty quantification [72]. A schematic of the software integration is shown in Figure 4.1. CFD-DEM will be simulated for various API and carrier particles size. For example, in jet nebulizer particle delivery method, budesonide particle size of 3.8-5.5 μm [73] at 1.3±0.1 g/cm^3 are used via liquid-air particle distribution mechanism whereas in DPI, API particle sizes between (1–5) μm [74] are used via solid particle-air mechanism.

4.4 Framework to Incorporate MFiX with Dakota

An interface between MFiX and DAKOTA is created via a C++ wrapper which can be seen in Fig. 4.1 [75]. This C++ wrapper is used to exchange the information between DAKOTA and MFiX and DAKOTA is the primary driver in this current framework, which generates values of uncertain input parameters. These values are used in making the input file for simulations with MFiX. The wrapper launches MFiX simulations and calculates the response functions. The response functions are returned to DAKOTA for calculating the low order statistics of the response functions. In DAKOTA input file, we define the parameters with uncertainty and their range. Besides, response functions and a UQ method to be employed are also specified in this input file.

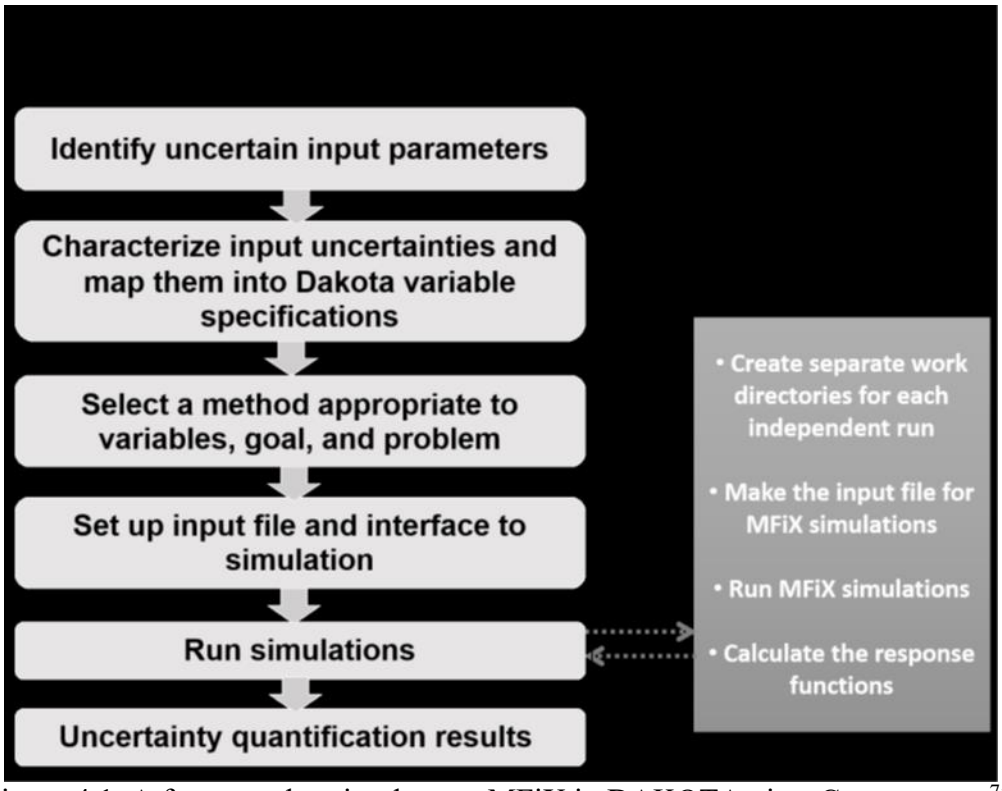

Figure 4.1: A framework to implement MFiX in DAKOTA via a C++ wrapper[75].

The wrapper creates a directory for a sample point or each independent run and makes the input file for MFiX simulations. The MFiX input file includes the values of the uncertain input parameters from DAKOTA. The values of these parameters are based on the upper and lower bounds and the probability distribution function. The wrapper launches MFiX executable for each sampling point and calculates the response function(s) when the input file for MFiX simulations is made.

The response functions derived at the end of MFiX simulations for all the sampling points are used to calculate the low order statistics with DAKOTA. The C++ wrapper is integrated with DAKOTA via the fork interface. The fork/exec interface in DAKOTA return a process identifier that the wait functions can use to detect the completion of a simulation for either synchronous or asynchronous operations. The interface avoids the potential of a file race condition when

employing asynchronous local parallelism. This condition can occur when the responses file has been created, but the writing of the response data set to this file has not been completed. It has additional asynchronous capabilities when a function evaluation involves multiple analyses. The fork interface supports asynchronous local and hybrid parallelism modes for managing concurrent scans within function evaluations.

4.5 ANSYS:

The numerical analysis of fluid flow gives us an extensive idea of the Computational Fluid Dynamics (CFD), which becomes a great concern to engineers and scientists. CFD owes its popularity for predicting fluid flow, heat transfer, and chemical species transport in different environmental condition analysis [76]. With the advent of powerful parallel computers and advances in computational techniques in recent years, CFD gives quantitative and qualitative analysis of fluid flow that is able to deal with the real life problems with better accuracy [77].

In this numerical analysis-based work, several cases for different particle size and different velocity on a DPI device will be discussed. To get the best aerosol particle delivery into the pulmonary system, a comparison needs to be made based on all the particle and flow parameters. It would take a huge cost to check all these cases in practical life. Therefore, numerical analysis provides a guideline to choose the best experimental setup to make it more cost effective [78].

The flow field inside DPI is a complex phenomenon in fluid dynamics problem. A combined approach on CFD and discrete element method (DEM) is exhibited on this project which explains the particle-particle and particle-fluid interactions [79-90]. For better understanding of complex particle-fluid flow, CFD–DEM approach has been extended in several studies on the gas–solid flow on inhaler device [91-95]. CFD analyzes the fluid dynamic phenomena by using numerical methods. Fluid Dynamics (FD) solution can be obtained by sets of governing equation.

Navier–Stokes equation controlled the gas phase simulation in CFD–DEM modelling [96]. The Navier–Stokes equations are nonlinear partial differential equations that illustrates the conservation of linear momentum for a linearly viscous (Newtonian), incompressible fluid flow [97, 98]. Density does not vary with the fluid motion in an incompressible flow.

4.5.1 Grid Generation

Grid is generated in ANSYS WORKBENCE software for the CFD solver. Discrete domain with grid can replace the continuous domain for CFD simulation. In continuous domain, each flow function can be outlined at every point of the domain. On the other side, each flow function is defined at the grid points only in discrete domain. The discrete system is a set of coupled, algebraic equations in the discrete variables. Discrete system includes a very large number of iterative calculations which is done by the digital computer. Figure 4.2 shows the pressure (p) variable in 1D continuous and discrete domain. It can be said from the figure that the pressure would be defined only at the N grid points in terms of discrete domain where, $p_i = p\ (x_i);$ i = 1; 2; N and for continuous domain, it would be, $p = p(x);\ 0 < x < 1.$

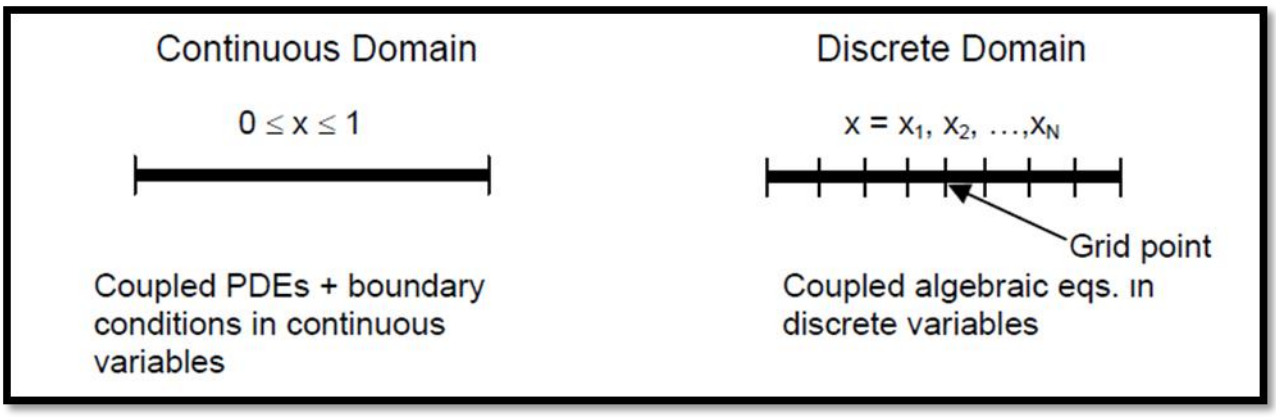

Figure 4.2: Examples of continuous domain and discrete domain

Grid, a discrete geometrical representation, divides the computational domain into cells or elements on which the flow and differential problem can be solved in a most accurate and effective

way. Success of the CFD analysis lies on the design and construction of a quality grid. Solution accuracy and rate of convergence is dependent on the grid size. Higher accuracy can be obtained by building finer mesh. Coordinate system gives points and directions to make a grid point. Cells are grouped into boundary zones where B.C.s is applied. Structured and unstructured, both grids are used on computational domain. Structured grid can't be used on complex geometries. A regular pattern grid arrangement is called structured grid, while irregular pattern arrangement is called unstructured grid. Unstructured grid is commonly used with the finite element method. We have used structured hexahedral grid on this dissertation. Depending on the solver capability and problem settings, different types of grid are used on numerical analysis. Both 2D and 3D grid can be generated in ANSYS software. 2D grid takes less memory and less time to perform numerical analysis. A 2D grid usually considers no velocity gradients in the direction normal to the grid. 3D grid generation is the most time consuming part of the 3D simulation calculation. It takes longer computational time than 2D grid generation.

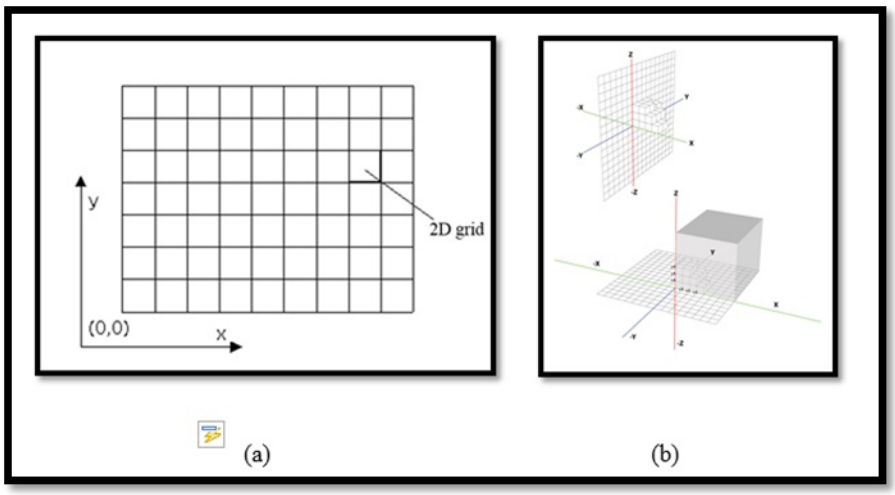

Figure 4.3: Different types of grid (a) 2D grid, (b) 3D grid

Governing equations are not good enough to get analytical solutions of fluid flow or heat transfer problem. Finite volume method can solve the partial differential equations on fluid flow

analysis. To analyze fluid flow inside a computational domain, the domain is discretized into smaller volumes or subdomains. Then the governing equations solve every discretized volume. These discretized subdomains are called elements or cells and the set of all elements are called mesh. Appropriate choice of mesh will impede the simulation error and can give us an accurate result during the flow analysis in Fluent.

4.5.2 Numerical Modeling

A highly reliable CFD modeling can help us to understand the physics inside the flow field of DPI sampler. Appropriate computational modeling is essential to comprehend the flow physics of the system and determine the underlying methodology of CFD. It can accurately predict the behavior of flow with the help of powerful digital computers. The numerical solution of computational flow modeling includes resolving the fluid dynamics phenomena in details. Grid refinement is important to determine the ordered discretization error in CFD simulation. Computational problem size can be augmented by grid refinement which will increase the need for parallel computing. The multiphase flow considered here is isothermal system which does not involve temperature change, even though temperature variation could play a role to change the deposition of particle inside the tube. The flow is 3D incompressible gas-droplet/particle two-phase interactions.

Turbulence models are based on statistical analysis as it is becoming an interesting alternative on CFD modelling. In past years, different turbulent models, e.g. standard $k-\epsilon$ model, $k-\omega$ model, and RNG $k-\epsilon$ have been applied to RANS to model DPI flow inside the separator/sampler [99]. Large disparate results compared to experimental data have been reported in published literature (e.g. Chen 1997). For this reason, different turbulent models have been

justified for DPI flow as a first step of the design evaluation. On the other hand, the numerical simulation efficiency mainly depends on the form of the turbulence modelling. As standard k–ε turbulence model conducts to impracticable tangential velocities and enormous turbulent viscosities, previous studies indicate the inability of standard k–ε turbulence model to simulate the highly swirling turbulence flow [100]. Since Reynolds stress turbulence model (RSTM) justifies the stream curvature effects, rotation and the swirling flow effects, this (RSTM) model is appropriate for highly anisotropic flows. But to observe a simple, smooth flow field inside fluidized bed, Laminar model is used in this case. Velocity fluctuation profiles will describe fundamental mechanism inside the fluidized bed.

4.5.3 Mathematical Modelling:

Computational fluid dynamics (CFD) method is used to model the performance of a DPI and it can anticipate the flow field characteristics and the particle trajectories inside the inhaler. The intricate turbulent flow in a DPI places great demands on the numerical techniques and the turbulence models employed in the CFD codes when modelling the DPI performance.

FLUENT uses a finite volume method (FVM) to solve the governing equations. Reynolds-averaged Navier-Stokes equations (RANS) for steady and incompressible fluid flow can be expressed as:

$$\rho u_j \frac{\partial u_i}{\partial x_j} = -\frac{\partial p}{\partial x_i} + \frac{\partial}{\partial x_j}\left[\mu\left(\frac{\partial u_i}{\partial x_j} + \frac{\partial u_j}{\partial x_i}\right)\right] + \frac{\partial \tau_{ij}}{\partial x_j} \tag{4.13}$$

$$\frac{\partial u_i}{\partial x_i} = 0 \tag{4.14}$$

where, the superscripts i, j = 1, 2 represent the Cartesian coordinate system components, $\rho, u, p \; and$ μ is the fluid density, velocity, pressure and viscosity respectively and

$$\tau_{ij} = -\rho\overline{\acute{u}_i \acute{u}_j} \tag{4.15}$$

which is defined as the Reynolds stress tensor that indicates the turbulent fluctuations effects on the fluid flow. The dash and overbar represent the fluctuating part and a Reynolds average term.

Reynolds stress model

The standard k-ε model is inappropriate due to its certain limitations in the case of strong swirling flow [101]. Reynolds stress model (RSM) can solve the transport equations of Reynolds stress model within particular stress components and improves the isotropic turbulence of k- ε model. The transport equations of Reynolds stress (RSM) model can be written as follows:

$$\frac{\partial \rho u_i u_j}{\partial t} + \frac{\partial}{\partial x_k}\left(U_k \partial \rho \overline{u_i u_j}\right) = P_{ij} + \emptyset_{ij} + \frac{\partial}{\partial x_k}\left[\left(\mu + \frac{2}{3}\, c_s\, \rho \frac{k^2}{\varepsilon}\right)\frac{\partial \rho \overline{u_i u_j}}{\partial x_k}\right] - \frac{2}{3}\delta_{ij}\varepsilon\rho \tag{4.16}$$

where, k is the turbulent kinetic energy, ε is the dissipation rate of k, pressure-strain correlation is expressed in $\emptyset_{ij}$ terms and P_{ij} is the production term of $\overline{u_i u_j}$ which can be written as follows:

$$\mathrm{P} = -\rho\,(\overline{u.u}(\nabla U)^T + (\nabla\, U) \tag{4.17}$$

The turbulent dissipation rate presents within the individual stress equations. The equation for the turbulent dissipation rate ε is given as:

$$\frac{\partial \rho \varepsilon}{\partial t} + \nabla.(\rho\, \mathrm{U}\varepsilon) = \frac{\varepsilon}{k}(c_{\varepsilon 1} P - c_{\varepsilon 2}) + \nabla.\left[\frac{1}{\sigma_{\varepsilon RS}}\left(\mu + \rho C_{\mu RS}\frac{k^2}{\varepsilon}\right).\varepsilon\right] \tag{4.18}$$

The model constants in these equations are

$$c_s = 0.22;\ c_{\varepsilon 1} = 1.45; c_{\varepsilon 2} = 1.9; c_{\mu RS} = 0.115$$

Model Equations for Particle Motion

The equation of dispersed particles motion can be by integrating the force balance equation in a Lagrangian reference frame. FLUENT anticipates the trajectory of a discrete phase in a Lagrangian reference frame [102]. The force balance equation of a single dispersed particle can be written (for the x direction in Cartesian coordinates) as

$$\frac{du_p}{dt} = F_d\,(\mathrm{u} - \mathrm{u_p})\frac{g_x\,(\rho_p - \rho)}{\rho_p} + \mathrm{F_x} \tag{4.19}$$

where, F_x is an additional acceleration term , u is the fluid phase velocity, u_p is the particle velocity, ρ_p is the density of the particle, g_x is the gravitational acceleration and $F_d\,(u-u_p)$ is the drag force per unit particle mass where F_d can be written as [49]:

$$F_D = \frac{18\mu}{\rho_p {d_p}^2} \frac{C_d}{24} Re \quad (4.20)$$

Here, μ is the molecular viscosity of the fluid, ρ is the fluid density, d_p is the particle diameter and drag coefficient C_d can be determined by Morsi and Alexander's correlation. Re is the relative Reynolds number, which is defined as,

$$Re = \frac{\rho\, d_{p|u_p - u|}}{\mu} \quad (4.21)$$

Saffman's Lift Force

The Saffman's lift force (lift due to shear) can also be included in coupled force term. The Saffman lift force is a generalization form from Li and Ahmadi which can be written as:

$$\vec{F} = \frac{2Kv^{1/2}\rho dij}{\rho_p d_p (d_{lk} d_{kl})^{1/4}} (\vec{v} - \vec{v}p) \quad (4.22)$$

where, k = 2:594 and d_{ij} is the deformation tensor. This form of the lift force is intended for small particle Reynolds numbers.

4.5.4 BOUNDARY CONDITIONS

Boundary conditions (BC) are a set of conditions that specify the flow and thermal variables at the boundary of its domain. These are verily important parameter for the mathematical model and FLUENT simulations [103]. Without appropriate boundary condition settings, numerical simulation would not be able to solve the flow analysis. CFD requires proper boundary condition on the outer and inner surfaces of the fluid domain, while the inner surfaces represent fluid-structure interfaces [104]. In general, boundary conditions are two types i.e.

i. **Dirichlet boundary conditions** – specify the value of the variable at the boundary, e.g. $u(x) = constant$

ii. **Neumann boundary conditions** – specify the gradient normal to the boundary of the variable at the boundary, e.g. $\partial_n u(x) = constant$

iii. **Robin boundary conditions-** specify a linear combination of the values of a function and the values of its derivative on the boundary of the domain on an ordinary or a partial differential equation. If Ω is the domain of a given equation to be solved and ∂Ω represents its boundary, then the Robin boundary condition can be expressed as: $au + b\frac{\partial \mathrm{u}}{\partial \mathrm{n}} = g \quad on\ \partial\Omega$ where, a and b are some non-zero constants /wand a given function g defined on ∂Ω, ∂u/∂n is the normal derivative at the boundary and u is the unknown solution defined on Ω.

Usually boundary conditions depend on the type of analysis (incompressible or compressible). Another type of boundary condition is used to analyze fluid dynamics problem is called mixed type boundary conditions. These types of boundary condition specify a function of the form $au(x) + b\partial_n u(x) = constant$ at the boundary. Proper boundary conditions give an accurate solution of numerical simulation. Boundary conditions used at each face of each computational domain. It specifies physical conditions (e.g. solid wall, symmetry plane, etc.) in the boundary region and interfaces between contiguous or overlapped domain [105]. Inaccurate boundary condition settings can lead to a nonphysical simulation results. Therefore, defining proper and effective boundary condition is the most important part of CFD analysis.

For this research, we have used four different boundary conditions, i.e., velocity inlet at inlet, pressure outlet at outlet, wall for boundary wall and interior BC for the interior zone. As discrete phase calculations are accountable in this work, so discrete phase conditions will be included in every boundary conditions.

i. **Velocity inlet:** Velocity inlet BC defines the velocity vectors and scalar properties of the flow at flow inlets. Since the total (or stagnation) properties of the flow are not fixed, their values may vary to give the recommended velocity distribution.

ii. **Pressure Outlet:** Pressure Outlet BC is used when the flow velocity and pressure are known before. Other flow variables are extrapolated from the interior. This boundary condition requires the specification of a static (gauge) pressure at the outlet boundary. The value of the specified static pressure is used only for subsonic flow. In case of supersonic flow, the specified pressure will no longer be used; instead the pressure will be extrapolated from the flow in the interior.

iii. **Wall:** Wall BC is used to bound fluid and solid regions. No-slip BC is implemented on the wall in viscous flow. Based on flow field details inside the computational domain, the shear stress and heat transfer between the fluid and the wall are calculated.

iv. **Interior:** Interior BC is used on flow fluid through an area.

4.6 Tensorflow

TensorFlow is an open source library that uses dataflow graph to represents a computation. It was developed by the Google Brain team for implementing and distributing large-scale machine learning models [106]. It supports a broad range of models efficiently including other types of learning algorithms by distributing computations across thousands of multi-GPU servers and used in computer vision, speech recognition, natural language processing, and text mining. Nodes in the dataflow graph shows numerous *operations* including mathematical functions such as addition and matrix multiplication; constant, sequence, and random operations for initializing tensor values; summary operations for producing log events for debugging; and variable operations for storing model parameters [107]. Therefore, TensorFlow is an interface for machine learning algorithms and an application for implementing such algorithms on various heterogeneous systems.

C++ wrapper creates an interface between TensorFlow and DAKOTA. This wrapper interchanges the data among DAKOTA and TensorFlow. DAKOTA creates uncertain input parameters values and provides those to TensorFlow. The wrapper launches TensorFlow and guides the machine learning algorithm with the data created from DAKOTA-MFiX simulations [75]. Then the algorithm predicts the quantities of interest (QoIs) for the dataset. The wrapper go back to the predicted values and DAKOTA connects the wrapper through the fork interface. The wrapper invokes TensorFlow or MFiX via the system functions. A framework to integrate DAKOTA with TensorFlow is shown in Figure 4.4.

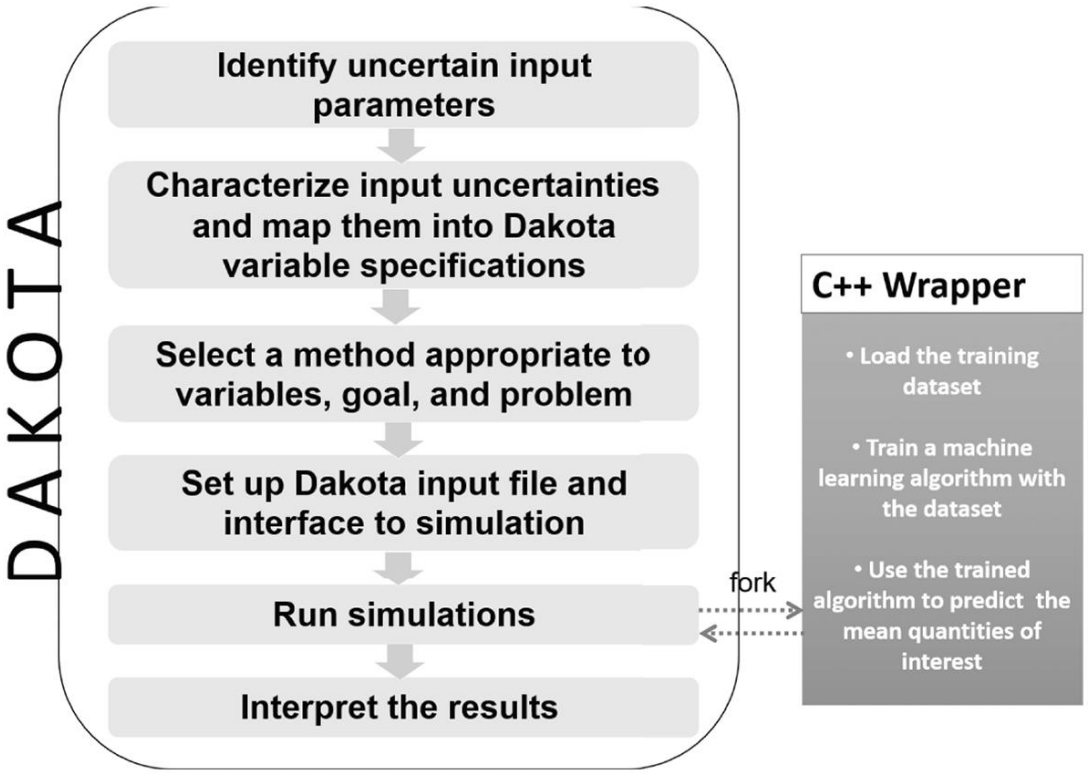

Figure 4.4: A framework to implement TensorFlow with DAKOTA via a C++ wrapper[75]

4.8 Summary

A novel high fidelity CFD discrete element modeling (CFD-DEM) method and sensitivity analysis will be used for predicting the transport and deposition as well as the agglomeration and

deagglomeration for DPI carrier and API particles. The CFD-DEM algorithm models agglomeration and deagglomeration forces with MFiX. A model validation with available data from the literature for DPI needs to be done with MFiX and ANSYS code and a sensitivity analysis of various formulation properties and their effects on particle size distribution needs to conduct with DAKOTA. MFiX has been developed by National Energy Technology Lab for fossil energy applications and brings cutting CFD-DEM capabilities. Trilinos and DAKOTA have been developed by Sandia National Labs and bring state-of-the-art exascale capable portable and scalable linear solver and UQ capabilities. MFiX, Trilinos, and DAKOTA are open source software and written for exploiting High-Performance Computing capabilities of a massively parallel supercomputer, while ANSYS needs licensing for using it.

Chapter 5: Results and Discussion

We considered a fluidized bed with central jet in two dimensions. The flow in a fluidized bed of 15cm width 90cm height is simulated with DEM model in MFiX. Initially, the half of the bed is filled with sand particles of size 0.04cm and density of 2.7g/cm3. The void fraction at minimum fluidization of the bed is 0.42. The spherical particles of size 4mm are fluidized with air of density of 0.0012g/cm3 and viscosity of 0.00018Poise. The particle-particle restitution co-efficient is 0.9 while the particle-wall restitution co-efficient is 1.0. The stiffness co-efficient of particle is 800 N/m. The damping and friction coefficients of particles are 0.18 Ns/m and 0.3, respectively. The flow is assumed to be laminar as well as incompressible. The computational domain is discretized with 45 equi-spaced cells in the axial direction and 15 equi-spaced cells in the normal direction. Constant mass flow and pressure boundary condition is specified on the bottom and top boundary, respectively. The central jet velocity is 4200cm/s. The sparse linear system of equation resulted from the discretizing the Navier-Stokes equations with SIMPLE method are solved with Bi-Conjugate Gradient Stabilized (BiCGStab) method in MFiX. The flow (volume fraction) in the fluidized bed at time t=20 and t=30 is shown in Figure 5.1. The time histories of the bed height are also shown in the figure. The bed height (h) is defined at h(t) = $\sum_{n=1}^{N_p} Y^n / N_p$ where, N_p is the number of spherical particles and Y is the location of the particle in y-direction.

5.1: FLOW IN A FLUIDIZED BED WITH MFiX AND DAKOTA INTERFACE:

An interface between the MFiX and DAKOTA is created via a C++ wrapper for the uncertainty quantification of MFiX-DEM simulations. This wrapper exchanges the information among DAKOTA and MFIX–DEM for the uncertainty quantification. In the current framework, DAKOTA is the primary driver, i.e., it generates values of uncertain input variables via upper and

lower bounds and passes those input variables to MFiX-DEM via the wrapper and launches MFiX simulations. DAKOTA receives response functions from MFiX and preforms the uncertainty quantification. Then performs post-processing to extract the quantities of interest from MFIX–DEM results. In the input file for DAKOTA, we prescribe the variables with uncertainty and a range of values to determine the upper and lower bounds. In addition, the response variables with the type of uncertainty quantity analysis to be performed are also specified in this input files.

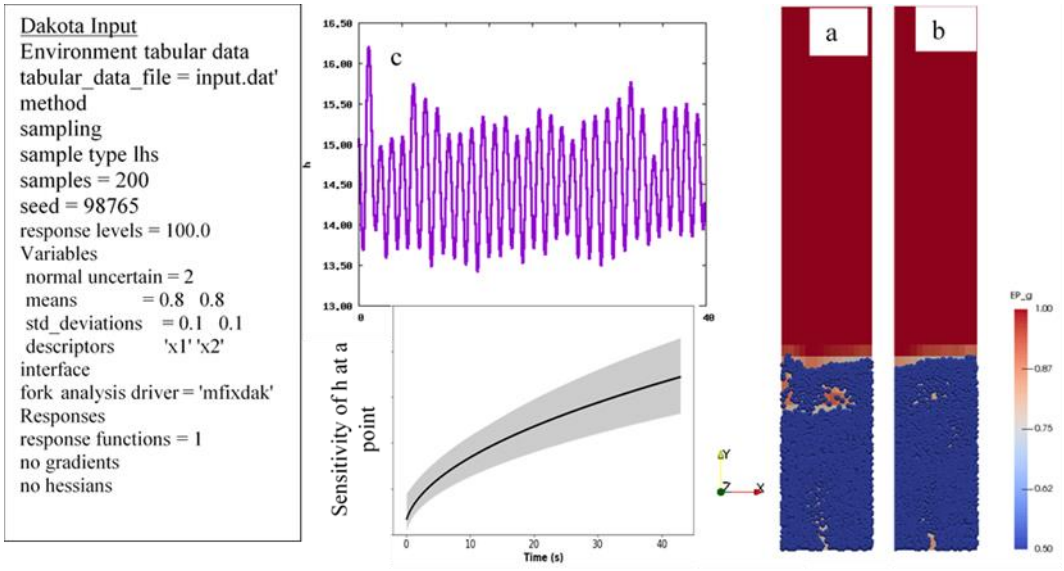

Figure 5.1: Flow in a fluidized bed with central jet: (a) Volume fraction fields at time t=20 (b) volume fraction fields at time t=30, and (c) time histories of the bed height

DAKOTA creates a directory for each independent run or a sample point and modifies the input file for MFiX simulations by substituting new set of values from DAKOTA for the uncertain variables considered in the MFiX-DEM simulations. The values for these variables are determined based on factors such as the sampling method chosen, number of samples, upper and lower bounds and the probability distribution function prescribed for the uncertain variable(s) in the DAKOTA input file. DAKOTA launches MFIX–DEM executable for each sample independently. The uncertainty quantification results with MFiX-DAKOTA framework for the fluidized bed with central jet having two uncertain input variables are listed in Table 5.1. The average bed height

decreases with the decrease in standard deviation of the input variables. Further, these results are in good agreement with the results from MFiX-PSUADE framework [54] where $e_{p,n}$ is the particle-particle restitution co-efficient and $e_{w,n}$ is the particle-wall restitution co-efficient.

Table 5.1: Monte Carlo (MC) simulations with different standard deviation specifications for input parameter distributions (based on 100,000 samples)

Case #	Input 1 $e_{p,n}$	Input 2 $e_{w,n}$	Avg. Bed height Sample mean	Avg. bed height Sample Std deviation
1	N(0.8,0.1)	N(0.8,0.1)	14.374	1.7e-01
2	N(0.8,0.05)	N(0.8,0.1)	14.331	7.5e-2
3	N(0.8,0.1)	N(0.8,0.05)	14.372	1.6e-1
4	N(0.8,0.05)	N(0.8,0.05)	14.330	7.5e-2

Figure 5.2 and 5.3 depict flow fields at time t=0.0s and 1.0s for different velocity directions. The particle movement in fluidized bed can also be seen in the figures. The initial location of the particles can be seen in the figures.

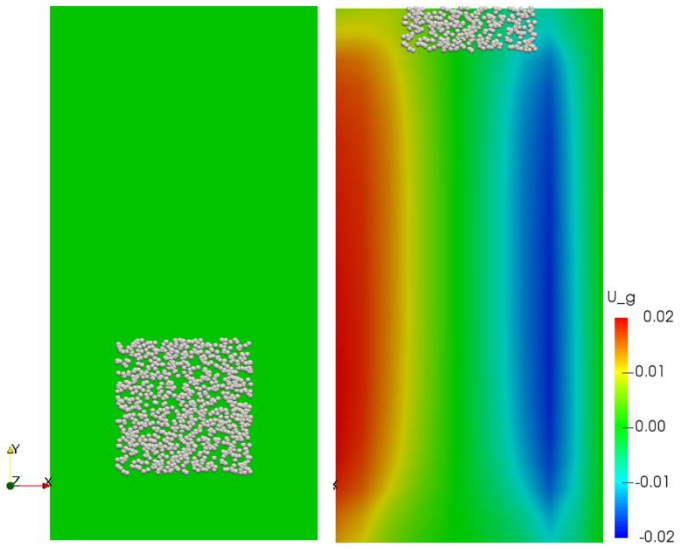

Figure 5.2: Flow in a DPI: Velocity along the x-direction fields at time t=0.0 s (left) and 1.0 s (right). The particles are shown with gray color.

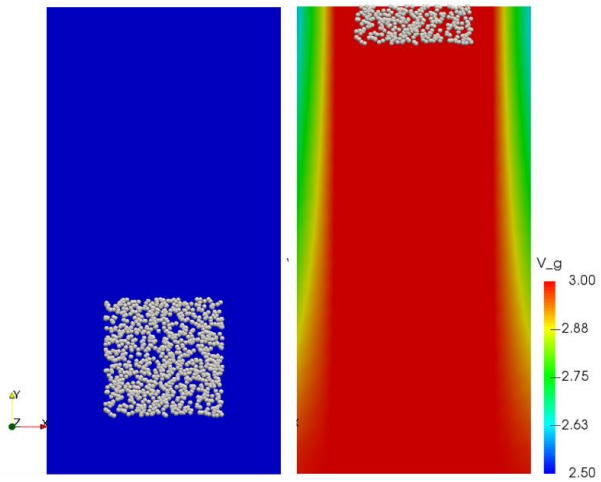

Figure 5.3: Flow in a DPI: axial velocity (y-direction) fields at time t=0.0 s (left) and 1.0 s (right). The particles are shown with gray color.

As the time progresses, the particles start to move towards the exit section or the top boundary and eventually exit through the outlet of the inhaler. At time t=1.0s, approximately half of the particles exited the inhaler.

Figure 5.4 shows the flow fields at time t=0.0s to 6.0s for axial velocity (y-direction) with different particle diameter than Figure 5.2 and 5.3. The particle movement in fluidized bed can be seen for different time frame. It shows that the bed was so cohesive at first that no fluidization occurred at t=0 s and all particles remained in the bed. At t=1 s, the agglomerated particle entrained into the airflow and the bed starts to fluidize. So, very little particle movement is observed at this time. But due to the cohesivity between particles, particle agglomeration with the flow becomes higher and more frequent. Therefore, packed particles are started to move faster and try to leave the domain. When the gas velocity exceeds the particle's terminal velocity, then the particle carried out of a bed at t=6 s. At this time half of the particle leave the inhaler.

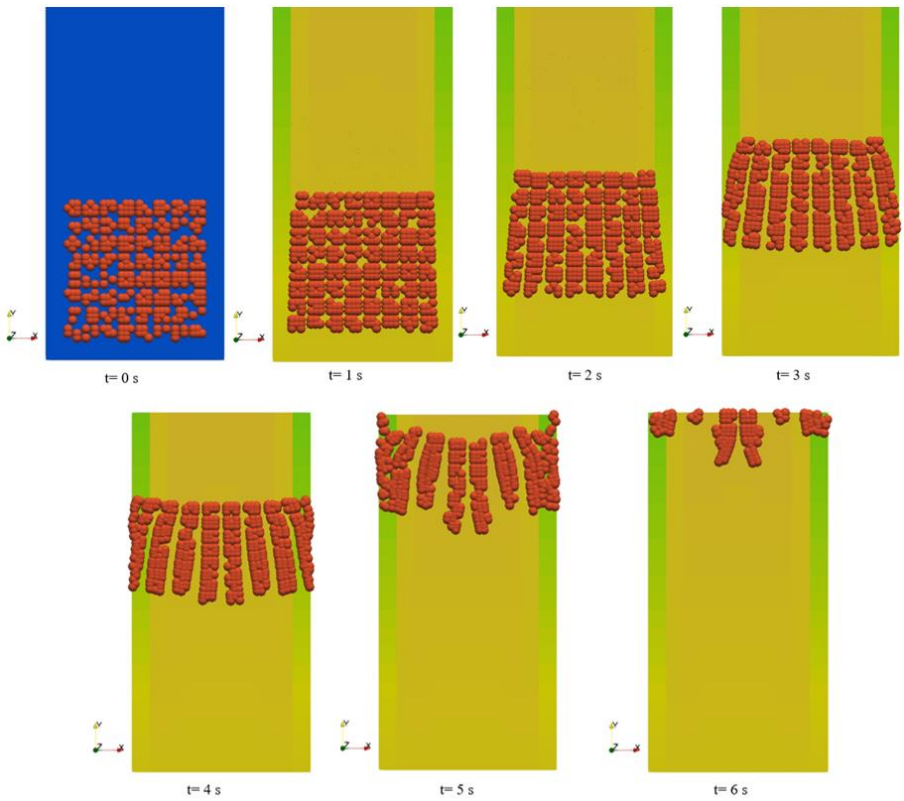

Figure 5.4: Particle movement as a sequence of particle agglomeration with time in a dry particle inhaler. The particles are shown with red color.

5.2: Effect of Particles Diameter

Particle size plays an important role in determining the possibility of aerosol particles in the lung. The particle residence time is dependent on the particle size, density, and fluidization velocity. For a given particle size and composition, this particle residence time usually larger than the total reaction time. Figure 5.5 and 5.6 depict the change of flow field's time with the change of particle size at a constant velocity. The particle movement in fluidized bed can be seen for different time frame, while the same fluidization velocity has been used in both cases. With the change of particle size at same fluidization velocity, the smaller particles leave the domain at 2 seconds while the larger particles take more time to leave the domain.

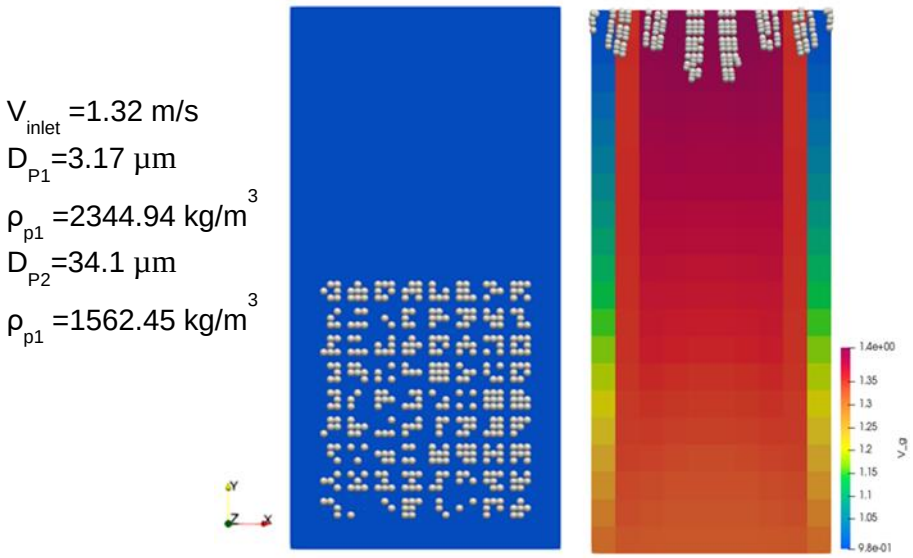

Figure 5.5: Flow in a DPI: axial velocity (y-direction) fields at time t=0.0 s (left) and 2.0 s (right). The particles are shown with gray color

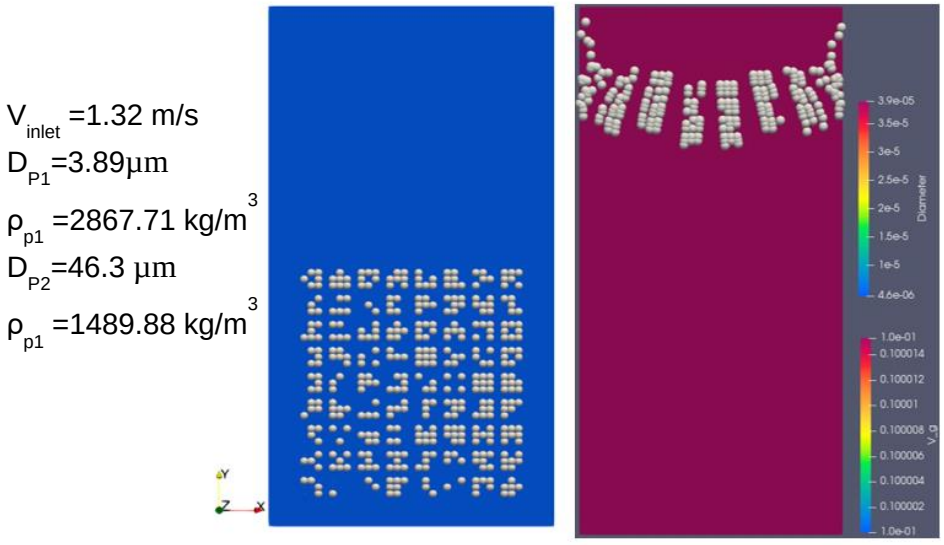

Figure 5.6: Flow in a DPI: axial velocity (y-direction) fields at time t=0.0 s (left) and 3.0 s (right). The particles are shown with gray color.

It is known that particles larger than 6 µm can pass the mucociliary clearance (MCC) in the ciliated region of the lung [108] and particles with diameters between 1 and 5 µm are preferably are suitable for inhalation and can reach upto alveolar macrophages in the alveoli [109]. But due

to the high surface free energy in smaller drug particles, they tend to stick together *via* cohesive forces or to any surface they run into *via* adhesive forces, show poor flowability and aerosolization performance and have an inclination to remain within the inhaler. To overcome these problems, carrier particles are used to improve the flowability of drug particles and increase the dispersion of drug particles during release by diluting the drug to improve accurate dose delivery. In this regard, several simulations have been run with a wide variation of drug and carrier particle size distribution to predict the optimal particle movement. After getting a wide range of data for various particle size distribution, a few are selected for analysis which is shown in Table 5.2. The main objective of this research is to obtain reproducible, high pulmonary deposition that can be highly provoked by physico-chemical characteristics of carrier.

Table 5.2: Particle residence time with change of drug particle and carrier particle size (Based on simulations running on MFiX)

Drug Particle Diameter, µm	Carrier Particle Diameter, µm	Residence Time, s
1.80	7.10	4
1.80	7.20	4
1.92	5.13	2
2.40	5.10	4
2.90	6.30	5
3.10	5.10	4
3.11	5.60	3
3.30	6.30	4
3.33	6.30	5
3.40	4.10	4
3.50	5.40	5
3.50	6.10	6
3.66	4.73	3
4.50	6.30	6
5.14	6.37	8

In this project, simulations have been done for different parameter. A particle size distribution is one of the parameters. This function should be included to accomplish optimal particle movement by controlling both the particle reaction time and residence time in the fluidized

bed environment. In this project, drug particles diameter starts from 1.8 to 5.14 μm and carrier particle diameter from 41 to 72 μm has been chosen based on previous research. So, this table is created from the data of lowest particle size to highest particle size and several simulations have been done with a wide variation of drug and carrier particle size range to observe which one shows better particle movement based on time. In first case, lowest drug particle size is used with highest carrier particle size and shows residence time of 4 seconds. But in 2nd case, same size of drug particle mixed with higher size of carrier particle than 1st case and shows comparatively higher residence time. Then 1.92 μm size of drug particle and 51.3μm of carrier particle only takes 2 seconds time to leave the fluidized domain and can react rapidly into target areas after inhalation. Also, 3.11 μm diameter drug particle and 5.6 μm carrier shows better residence time which means they can deliver the medication within a short time. In this study, larger carriers (90–125 μm) showed a higher drug dispersion than the same formulation with 38–60 μm carriers.

Based on all of the data from Table 5.2, Figure 5.7 is showing the particle movement timeframe based on particles size changes. From Figure 5.7, it can be seen that with the change of particle size, the particle residence time has been changed, which changes the time of medicine delivery into lungs. Smaller size of drug particle is chosen here, so they can reach deeper areas into the lung but their stronger adhesion to surfaces resulting in a greater loss of particles in the aerosol and also in the mouthpiece during inhalation. And larger carrier particles have larger surface discontinuities which gives cover to drug particles from the press-on forces during mixing [110]. For this reason, lowest size of drug and highest size of carrier particles have been chosen in 2nd case, though better results can be seen from other particle size distribution. Case #3 and #7 show the enhanced inhalation performance among all cases. Increasing size of drug and carrier particle reduces the inhaler performance by taking the higher residence time (in last case).

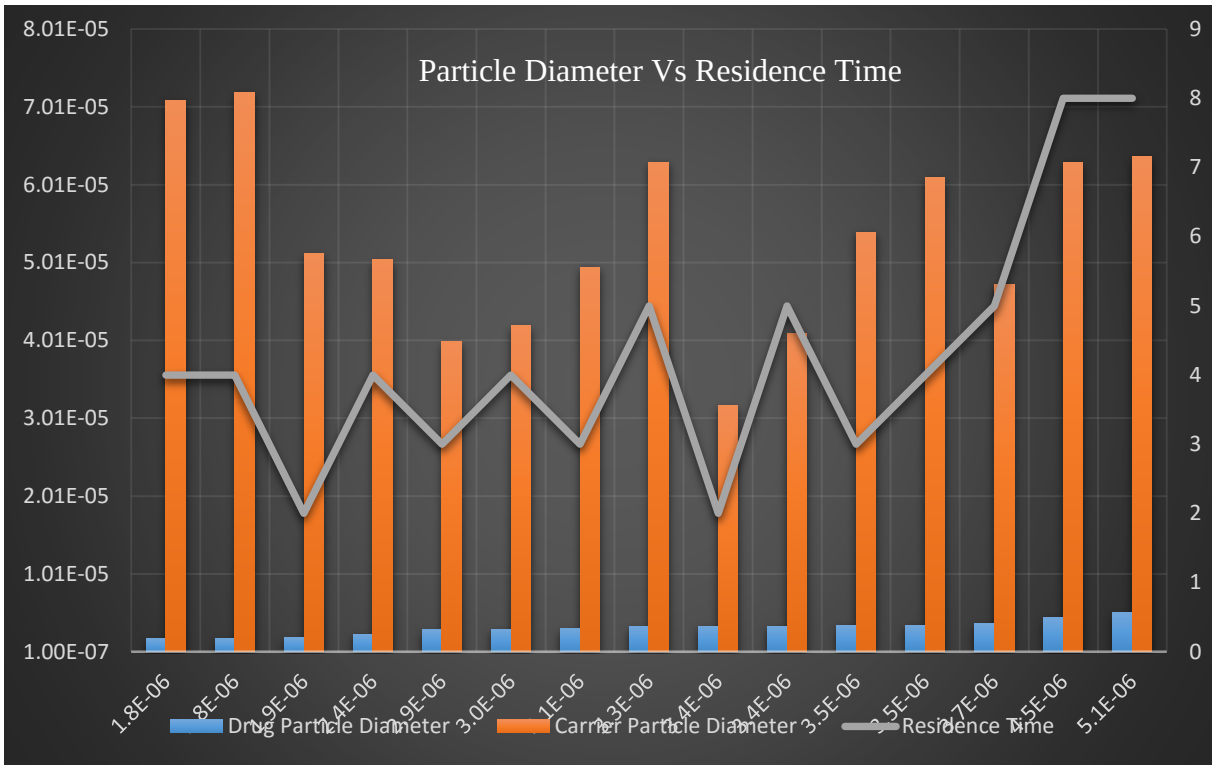

Figure 5.7: Particle Residence time with the change of carrier particle and drug particle size

As particles of 7.5 µm and larger mostly deposit in the oropharynx, whereas particles smaller than 0.5 µm may be exhaled again, so it is important to select ideal particle size that can deliver medicine into the respiratory tract with minimal time and act instantly. So it can be concluded that, drug particles of 1-3.66 µm show a higher drug dispersion and better aerosolization behavior with carrier particles between 51-63 µm.

5.3: Effect of inlet velocity change

Figure 5.8 depicts the change of flow field's time at a constant particle size with the change of velocity. Based on previous analysis, drug and carrier particle size is selected which have better aerosolization and higher drug dispersion rate. Two different fluid velocity has been chosen to see particle movement difference throughout the inhaler. The particle movement in fluidized bed can

be seen for different time frame with same particle size, while the different fluidization velocity has been used in both cases. With the change of fluidization velocity at same particle size, the particles with higher velocity leave the domain at 2 seconds while the same particles with less fluidization velocity take more time to leave the domain. This is because aerosol particles at higher fluidization velocity can better follow changes of air flow direction, thus moves fast. But such higher fluidization velocity results in more turbulence and eddy formation, which impedes the particle movement inside domain. So, inlet velocity of 2.5 m/s has been chosen as it shows reasonable results in terms of particle residence time.

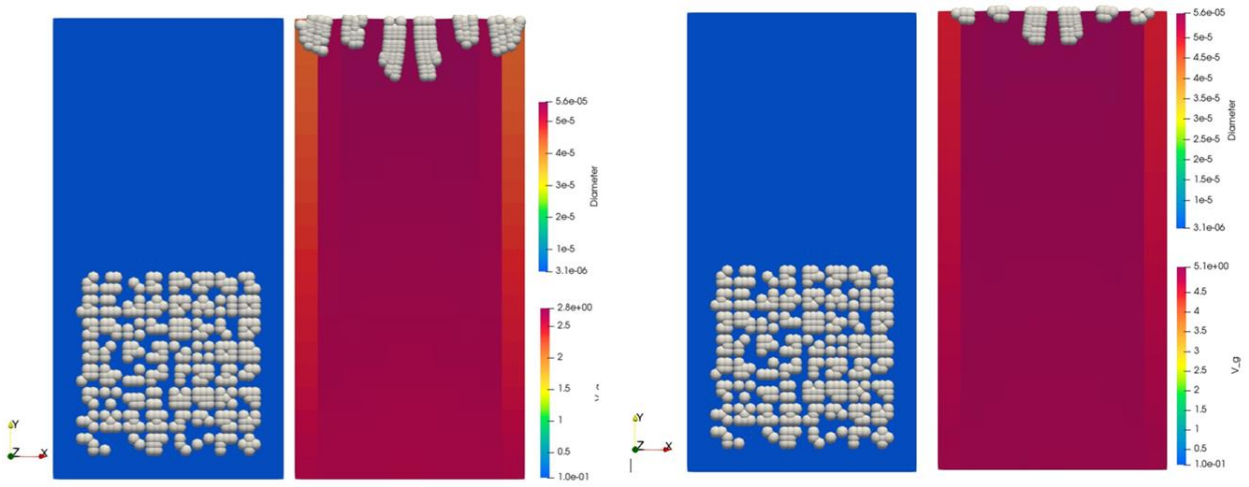

(a) (b)

Figure 5.8: Flow in a DPI: axial velocity (y-direction) fields for (a) at time t=0.0 s (left) and 3.0 s (right) at V_{inlet}=2.64 m/s and for (b) at time t=0.0 s (left) and 2.0 s (right) at V_{inlet} =5 m/s. The particles are shown with gray color.

As particle velocity influences the lung deposition, so the velocity at which the particle leaves the inhaler is very important. Consequently, selection of fluidization velocity is an important parameter in this project. It can been considered that particles (D (v, 2.5) of 3 µm), exhibit superior properties for leaving the inhaler.

5.4: Effects of Drug Particle on Lung Delivery:

After inhalation through DPI, the particle enters the respiratory tract and may deposited in different regions of the respiratory tract. Larger particles (>5 μm) could not follow the air streamline, so may deposit in these regions by impaction. In fact, deposition by impaction in the oropharyngeal region remains a major portion of the emitted dose for DPI devices. Contrariwise, small particles (<0.2 μm) can deposited in all regions of the respiratory tract by diffusion. Sedimentation is the major deposition mechanism in the small airways and alveolar region for inhaled particles. The effects of slip, shape and density on aerosol particle behavior is very important for delivering medications to the peripheral regions of the lungs. Slip correction factors for particles smaller than 10 microns, can derived by Cunningham are as followed:

$$Cc = 1 + Kn\left[A1 + A2\ exp\left(-\frac{A3}{Kn}\right)\right] \tag{5.1}$$

where, Kn is the Knudsen Number, and $A1$, $A2$ and $A3$ are constants. The values of these constants were determined in 1945 by Davies [109], and are given by Reist [110] and Hinds [111] as A1=1.257, A2=0.4 and A3=1.1.

Table 5.3 shows the change of Stokes number for a unit density sphere of a given particle size using slip correction with the constants. All values are calculated for atmospheric pressure. Particle settling velocity is also related to the slip correction factors. From Table 5.3, it can be seen that with the increase of particle diameter the drag forces decreases. Slip correction is significant for deposition of pharmaceutical aerosol particles. Particle deposition in lungs are dependent of particle size. Cunningham Slip Correction Factor is used to describe non-continuum effects for drag calculations on small particles. Without these correction factors, calculation of particle properties and deposition prospects would be inaccurate.

Table 5.3: Effect of Cunningham Slip Correction Factor on Stokes Drag and Terminal Settling Velocity (VTS)

Particle Diameter, μm	Cc	VTS (with Cc) m/s	VTS(without Cc) m/s
1.80	1.092180009	1.42E-04	1.30E-04
1.92	1.086418753	1.93E-04	1.77E-04
2.37	1.070010127	2.12E-04	1.98E-04
2.89	1.057413149	3.97E-04	3.75E-04
3.04	1.054580263	6.06E-04	5.75E-04
3.10	1.053523871	7.23E-04	6.86E-04
3.11	1.053351768	4.56E-04	4.33E-04
3.33	1.049827027	3.99E-04	3.80E-04
3.41	1.048658065	5.74E-04	5.47E-04
3.45	1.048093913	5.57E-04	5.32E-04
3.49	1.047542693	5.85E-04	5.58E-04
3.50	1.047406857	7.21E-04	6.88E-04
3.66	1.045334426	6.91E-04	6.61E-04
4.50	1.036872000	7.42E-04	7.16E-04
5.14	1.032280934	1.38E-03	1.33E-03

It can be said from the above table that particle deposition mechanism that have Brownian motion effects have shown low deposition efficiency for particles with the decreased slip correction value. For increment of particle size from 1.8 to 5.14 μm, drag force decreases thus terminal settling velocity increases when a slip correction factor is utilized. Smaller particles settle more quickly because of their smaller surface area cause less frictional drag force. For particles <5 micron, it is very important to correct for slip when calculating the settling velocity of these size of particles. When a slip correction factor is applied, then anticipated particle settling velocity increases. Since submicron particles are used here, so no drastic differences are visible between the corrected and uncorrected velocity values.

Figure 5.9 shows the difference of slip correction factor on particle diameter. Smaller size of drug particle have higher slip correction, which means these micron size particle has include effects of Brownian motion thus results in low deposition efficiency in the upper airways. The

resultant slip correction factor here is greater than unity and decrease linearly with particle size. When the particle size is 1.8 micron, then the slip correction factor is 1.092. With the increased particle size, the slip correction factor decreases and particle shows higher deposition efficiency in the upper airways. For this micron size particles, diffusion is always the dominating deposition mechanism. If diffusion coefficient is only due to diffusion, it is independent of particle density, because the diffusivity of particles is independent of particle mass.

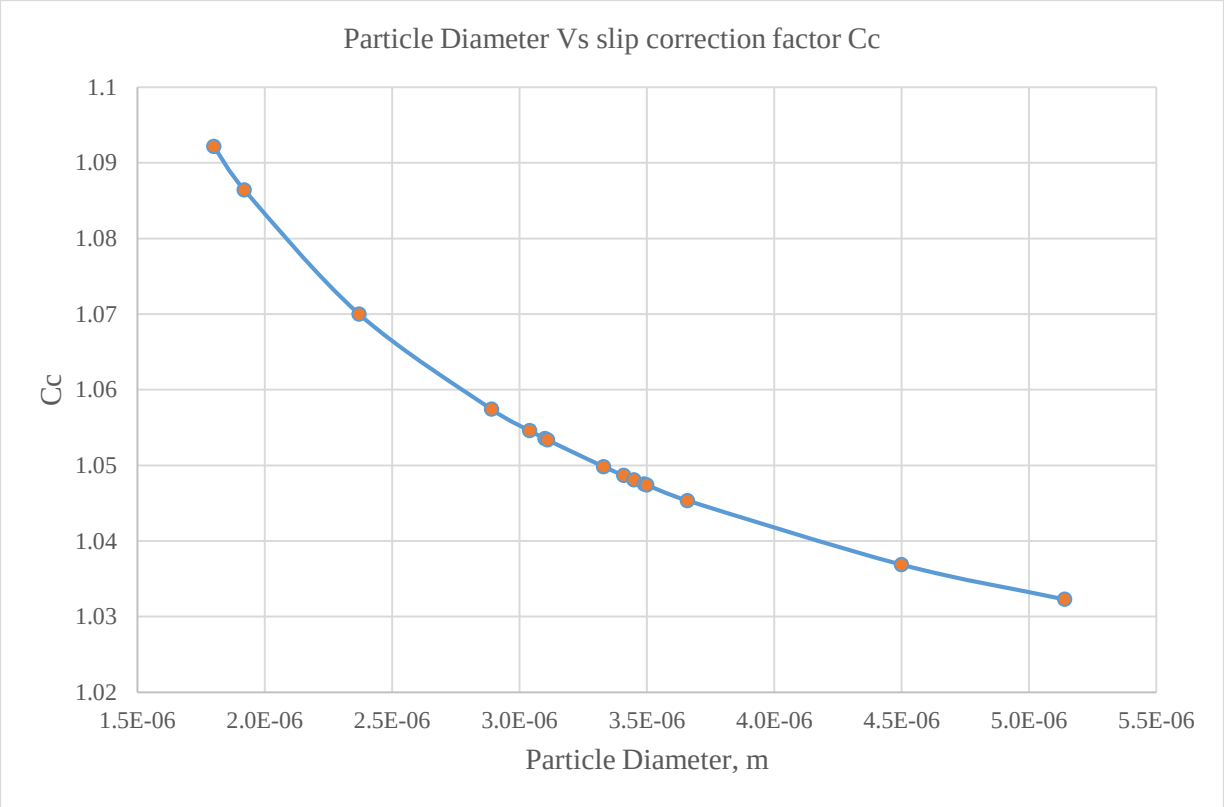

Figure 5.9: Difference of slip correction factor on particle diameter

Particles usually deposited due to inertial impaction and sedimentation. Particle deposition is directly dependent upon the relaxation time of the aerosol particle. Relaxation time describes the time required for a particle to adjust its velocity to a new state of forces. It indicates the particle's ability to acclimate quickly to a new condition. It depends on the mass and movement of

the particle, and is not influenced by the external forces acting on the particle [112]. Particle relaxation time can be expressed with following equations:

$$\tau = \frac{{d_p}^2 \rho_p}{18\mu} C_c \tag{5.2}$$

where, d_p is particle diameter, ρ_p is particle density, μ is air viscosity and C_c is Cunningham Slip Correction Factor.

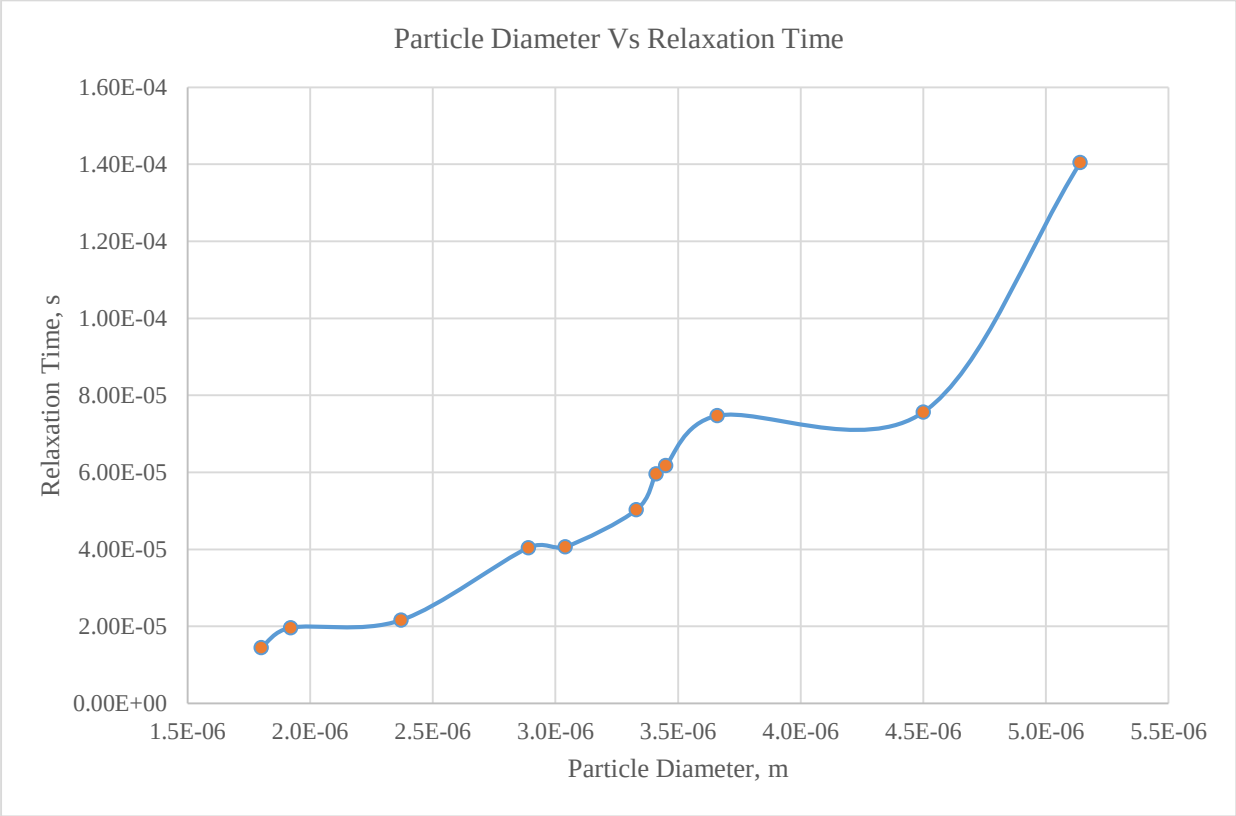

Figure 5.10: Relationship between particle relaxation time with the change of particle diameter

Figure 5.10 shows the relationship between particle relaxation time with particle diameter. The dimensionless relaxation time is usually used to understand the particle deposition in a fluid flow field. As relaxation time is proportional to the square of particle diameter, it increases rapidly with the increase of particle size. From the figure it is seen that, small particles have shorter relaxation time as they need less time to adjust to the fluid flow well. Smallest particle 1.8 μm took (14 μs) very short time to react with other particles and adjust into fluid flow. As particles become

larger in size, they tend to stick more to their primary track and took more time to react with other particles and adjust to flow field. So, it can be concluded that choice of smaller particle will be best for particle deposition in lungs.

5.5: Effects of Particle Size Distribution on Respiratory Track:

It is known from the previous studies that, larger particles between 10–15 μm deposit mostly in the upper airways while particles between 5–10 μm can reach the large bronchi, and particles of 1–5 μm penetrate to the lower airways and lung periphery [113]. So, it is important to define a desired particle size for better inhalation through inhaler device that can deliver the medications into targeted areas. For clinical use, inhaler devices can deliver polydisperse particle sizes i.e., mix of sizes in the aerosol particles. On the other hand, monodisperse aerosols consist of a single particle size, which are rare in nature and medicine.

A measure that calculates a polydisperse aerosol is the mass median diameter (MMD). This measure determines the particle size (in μm) above and below which 50% of the mass of the particles is surrounded [114]. This is the particle size that evenly divides the mass, or amount of the drug in the particle size distribution. The higher the MMD, the more particle sizes are of larger diameters.

The mass median diameter (mmd) is the most commonly used parameter for drugs inhalation in DPI device. The mass median diameter (mmd: the diameter above which 50% of the aerosol mass is contained) is a good parameter to define in this project, though the size fraction for which mmd is calculated should be defined also. Inhaled aerosols are usually defined by lognormal size distributions that are described by a mass median diameter (MMD) and geometric standard deviation (GSD) [115]. While these parameters generate statistics on relative proportions of

particle sizes, which mass distribution is more important, precisely describe the percentage of total mass from particles in the submicron range. Table 5.4 shows the particle size distribution defined by a mass median diameter (MMD).

Table 5.4: Particle size distribution defined by a mass median diameter (MMD)

Particle Diameter, μm	Density ,ρ (kg/m3)	Mass, Mi	MiDi	N	NiDi	NMD, μm	MMD, μm	GSD
1.80	1333.76	4.07282E-15	7.33E-21	500	9.00E-04	3.16	3.83	1.368
1.92	1596.94	5.91823E-15	1.14E-20	500	9.60E-04			
2.37	1170.09	8.15575E-15	1.93E-20	500	1.19E-03			
2.89	1491.32	1.88479E-14	5.45E-20	500	1.45E-03			
3.04	2065.09	3.0378E-14	9.23E-20	500	1.52E-03			
3.10	2372.08	3.70011E-14	1.15E-19	500	1.55E-03			
3.11	1485.85	2.34022E-14	7.28E-20	500	1.56E-03			
3.41	1562.41	3.24383E-14	1.11E-19	500	1.71E-03			
3.33	1136.94	2.19821E-14	7.32E-20	500	1.67E-03			
3.45	1483.5	3.18966E-14	1.10E-19	500	1.73E-03			
3.49	1521.99	3.38757E-14	1.18E-19	500	1.75E-03			
3.50	1866.24	4.18959E-14	1.47E-19	500	1.75E-03			
3.66	1639.36	4.2084E-14	1.54E-19	500	1.83E-03			
4.50	1173.52	5.59922E-14	2.52E-19	500	2.25E-03			
5.14	1677.66	1.19287E-13	6.13E-19	500	2.57E-03			
		Σ=5.11301E-13	1.96E-18	8000	2.53E-02			

All the calculations have been done based on previous data from this project. These findings will be beneficial to better understand the effect of micronized drug particle size into respiratory deposition. For a fixed MMD, the particle size range is greatly affected by the GSD. Mass of spherical particle is calculated by $M = \frac{\pi d^3 \rho_p N}{6}$, where N is the number of particle. For these selected particle size the mass median diameter is 3.83 μm. It means that particle with diameter of 3.83 μm evenly divides the mass, or amount of the particle in the particle size distribution. The higher the MMD, the more particle sizes are of larger diameters. For MMD of 3.83 μm, the GSD got is 1.368, the number median diameter (NMD) is 3.16 μm which is still into the submicron range, assuring that more than half of the particles are submicron in size. For particle size of 1.8 μm, the aerodynamic diameter is .66 μm. And for the highest drug particle size of 5.14 μm, the aerodynamic particle diameter is 0.044 μm. So, the aerodynamic diameter of all the particles are around 0.5 μm, which means they have the highest probability of depositing in the lung and the smaller sizes have greater probability to penetrate into the deep lung [116]. The larger the GSD value, the greater the spread of the aerodynamic diameters of the residual particles. So, for particles with relatively small MMDs (around 1-4 um), submicron particles considerably interject to pharmaceutical effect, but as MMAD increases, this effect is decreased.

5.6: Fluid Flow Visualization Inside DPI:

To study the air flow through the device a numerical simulation has been conducted by ANYS FLUENT. The geometry and standard settings kept same with MFiX simulations and 222111 rectangular cells was created to get a smooth visualization. The simulation was performed using discrete phase model for particle tracking. For better understanding the fluid flow inside the inhaler domain, contour and vector fields are important.

Figure 5.11 shows the velocity contour of fluid flow inside the computational domain. The air flow achieved a velocity of approximately 2.15 m/s when leaving the inlet and entering the inhaler domain. Particles are introduced into the domain with a very small velocity, which is negligible and cannot influence the fluid flow behavior anymore inside the domain. Due to no slip boundary conditions at wall surface, a minor velocity fluctuations is visible on both side of inhaler. But it stabilizes quickly with the flow. So, constant fluid velocity is observed throughout the domain.

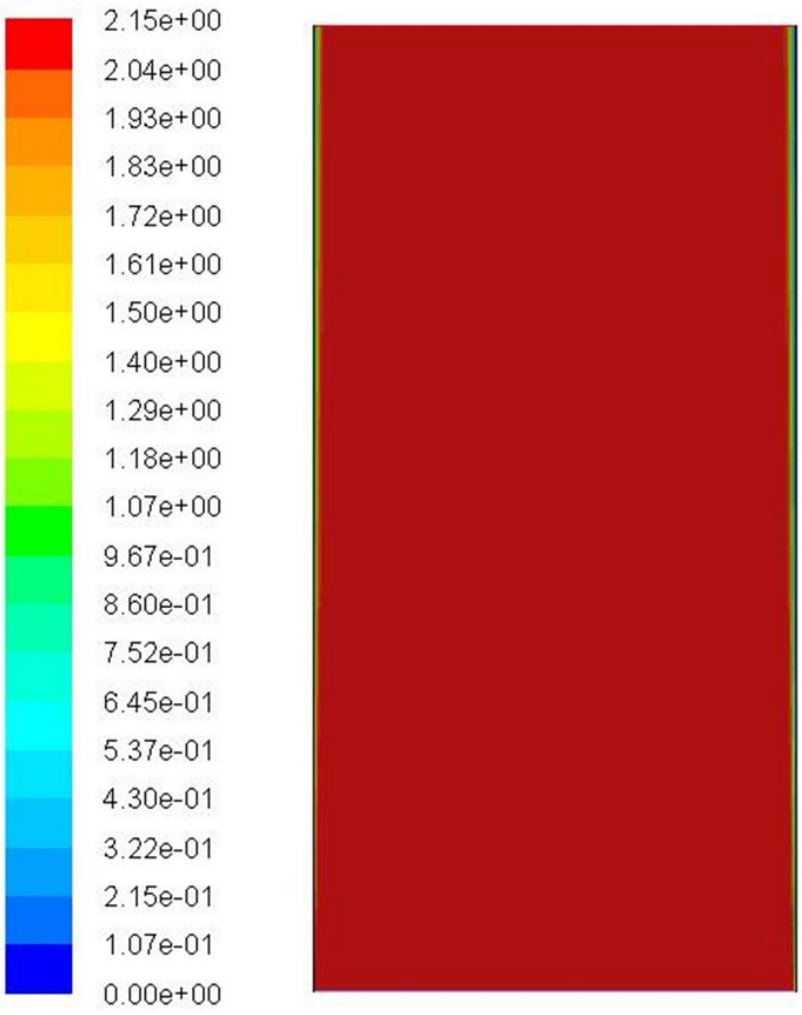

Figure 5.11: Velocity contour of air flow inside the computational domain

Figure 5.12 shows the velocity streamline of air flow inside the computational domain. Streamlines are a set of curves that are directly tangent to the velocity vector of the flow. It defines the direction that a fluid element travels in at any point in time. From the figure 5.12 it is seen that all the fluids are moving towards the outlet section. As particle are introduced to the flow field, few turbulence created in some region and the simulation shows little bit velocity fluctuations A little bit of flow fluctuation is visible near the inlet and wall regions as the particle velocity meets the fluid velocity but steadies quickly. But no reverse flow is observed through velocity field. Because of a smooth fluid flow with no backward flow inside the domain, all the particles can easily escape through the outlet.

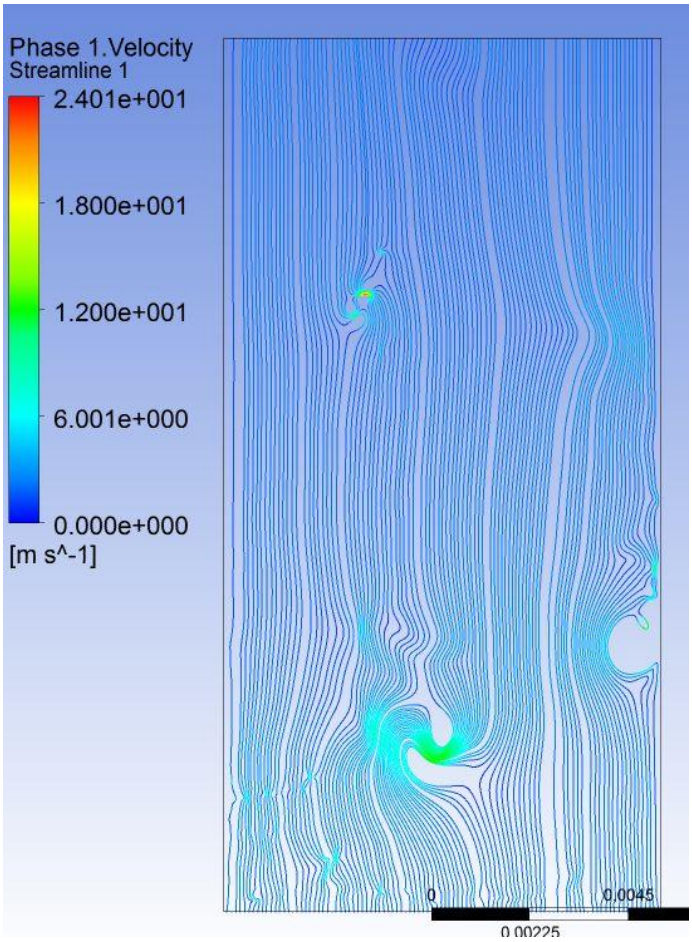

Figure 5.12: Velocity streamline of air flow inside the computational domain

Figure 5.13 shows the velocity streamline of particle inside the computational domain. All particle are introduced through the bottom inlet section. When particles mix with the fluid, their velocity increases in very small magnitude. This velocity fluctuation is small enough in the interior section, so it does not influence the flow behavior anymore inside the domain. Due to no slip boundary conditions at wall, particles may reflect into the fluidized bed and show a minor velocity fluctuations on both side of inhaler, which is negligible. But it stabilizes quickly with the flow. Because of no turbulence and eddy formation, particles can easily escape through outlet section on the top. So, a smooth flow behavior can be seen in the rest on domain which is good for efficient particle movement including escapes to the outlet.

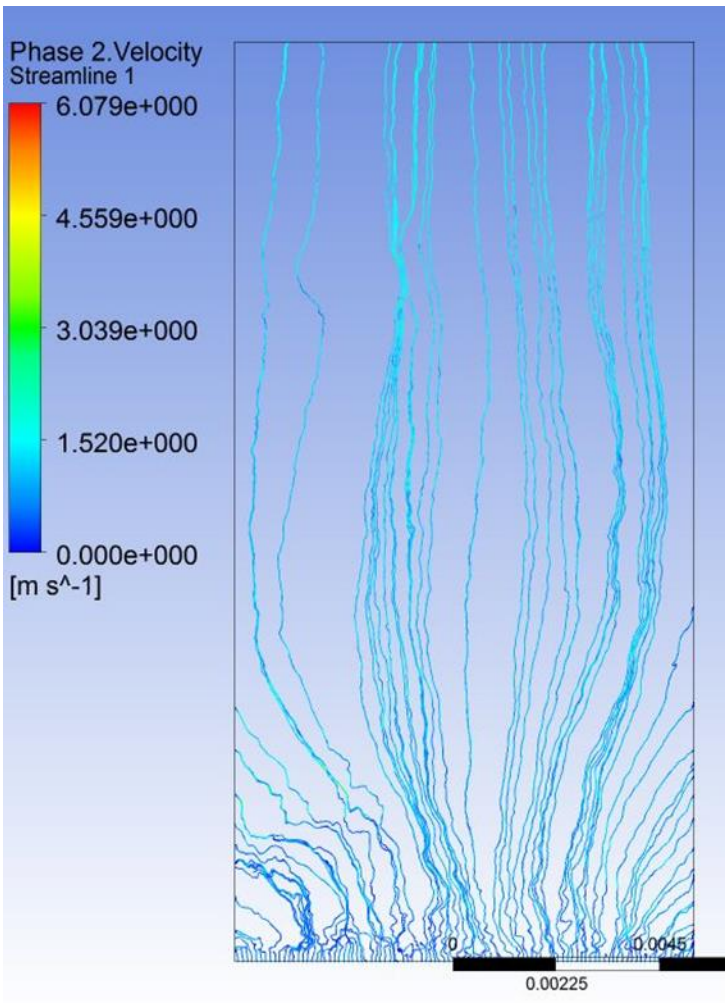

Figure 5.13: Particle velocity streamline inside the computational domain

5.7: Flow in A 3D Fluidized Bed with MFiX:

A 3D Eulerian-Lagrangian model has been simulated with the MFiX-PIC solver. Fluid is considered as a continuum while "parcels" represent groups of real particles with analogous physical characteristics. Figure 5.14 represents the gas velocity on MFiX 3D fluidized bed simulation from beginning to the end frame. 500 frames have been created during solving the whole simulation. It can be seen from the above figure that, at the beginning the gas velocity is constant as we implement to the simulation. As the particle enters the domain the gas velocity starts to change.

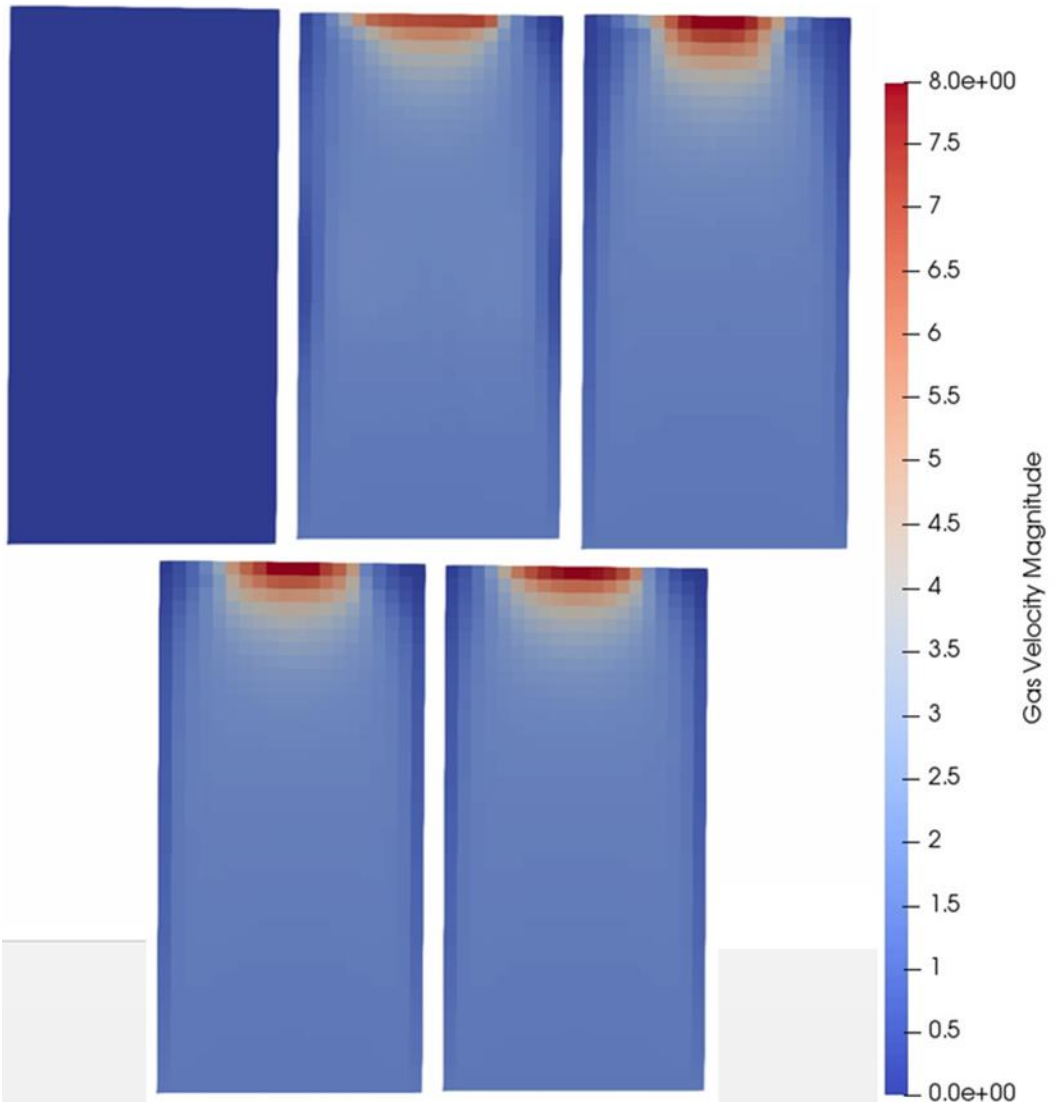

Figure 5.14: Gas velocity on MFiX 3D fluidized bed simulation from the beginning to end

Particles have their own (very small) velocity which mixes with the gas flow, so slight changes are visible in gas flow. Parcels movement is easily visible through the outlet section. Since the outlet section is constricted, so when the parcels exit the velocity becomes higher to that section. But overall, a slight variation is visible in gas velocity on 3D computational domain which is good for parcel movements.

Figure 5.15 depicts the fluid velocity in z-direction for 3D fluidized bed simulation. No significant changes can be seen through the fluid velocity in z direction. When the particles exit the outlet section, due to the constricted outlet section, high particle concentration occurs on that region. So, velocity changes in z-direction can be visible on outlet region. The lowest fluid velocity in z-direction is found at the outlet section. The velocity in z- direction decreases along with the height. The velocity is higher and it is almost constant near the bottom. This parameter can only be used in 3D cases to observe the flow field.

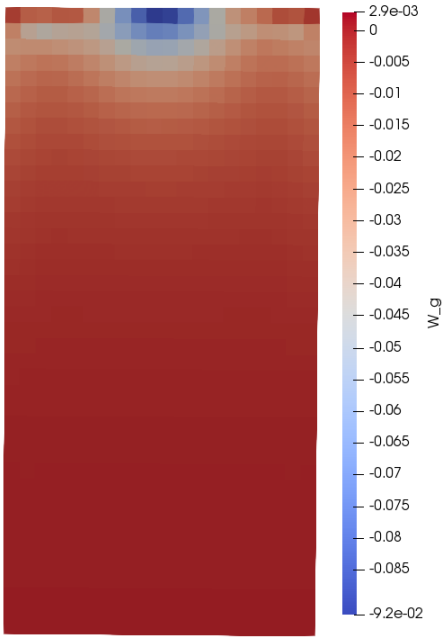

Figure 5.15: Velocity in z-direction on MFiX 3D fluidized bed simulation

Void fraction is an important parameter to define the gas-solid phase, denoted by εg for the fluid phase. This variable represents the amount of empty space between particles at each condition. Figure 5.16 depicts the void Fraction on MFiX 3D fluidized bed simulation. At the first

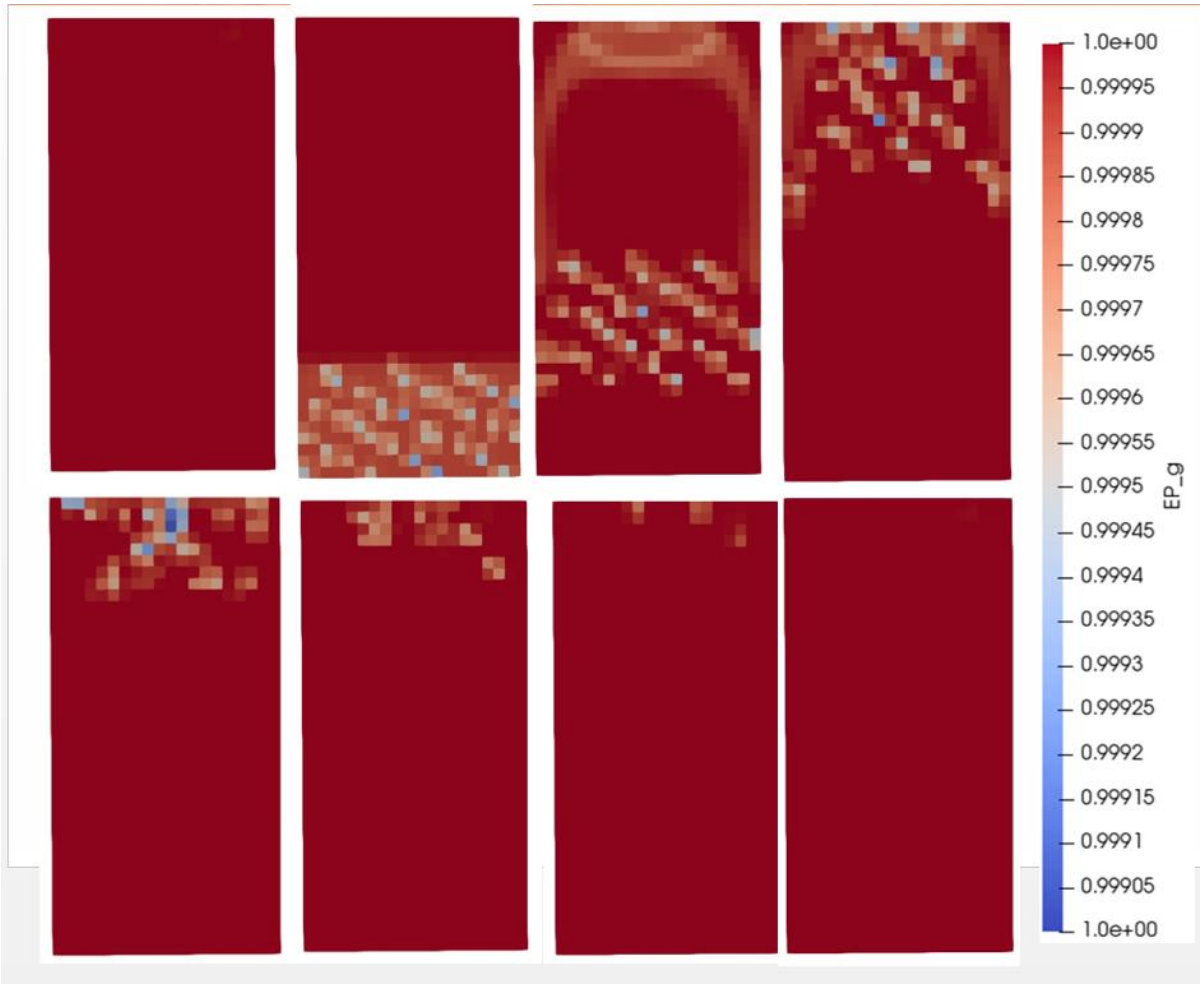

Figure 5.16: Void Fraction on MFiX 3D fluidized bed simulation

frame, no particle is present in the domain. So, the void fraction is magnitude of 1. As the particles introduced, the contours show low values of void fraction near inlet section. Due to parcle movement the void fraction decrease. As varying particle diameter is used in this 3D simulation, so with the parcel movemet the void fractions are changing. Therefore the void profiles are different with time frame.. The voidage profiles near the inlet section are identical showing a high

value near the bottom and low value near the top on figure 5.16(d). When all the parcel leave the domain, the void fraction in the domain becomes 1 again in figure 5.16(h). This fraction are used to analyze the gas-solid mixing and process efficiency.

Figure 5.17 shows the pressure field on MFiX 3D fluidized bed simulation. On figure 5.16(a), whole 3D domain with particles can be seen for pressure field. Red color represents carrier particles where blue ones are the drug particles. Particles are leaving through the outlet section on the left figure. Based on the real case scenarios, the pressure for the whole domain was chosen and it is ideal to maintain the whole domain at that constant pressure. No significant pressure change is observed on the computational domain. Better visualization of pressure field can be visible on figure 5.17(b).

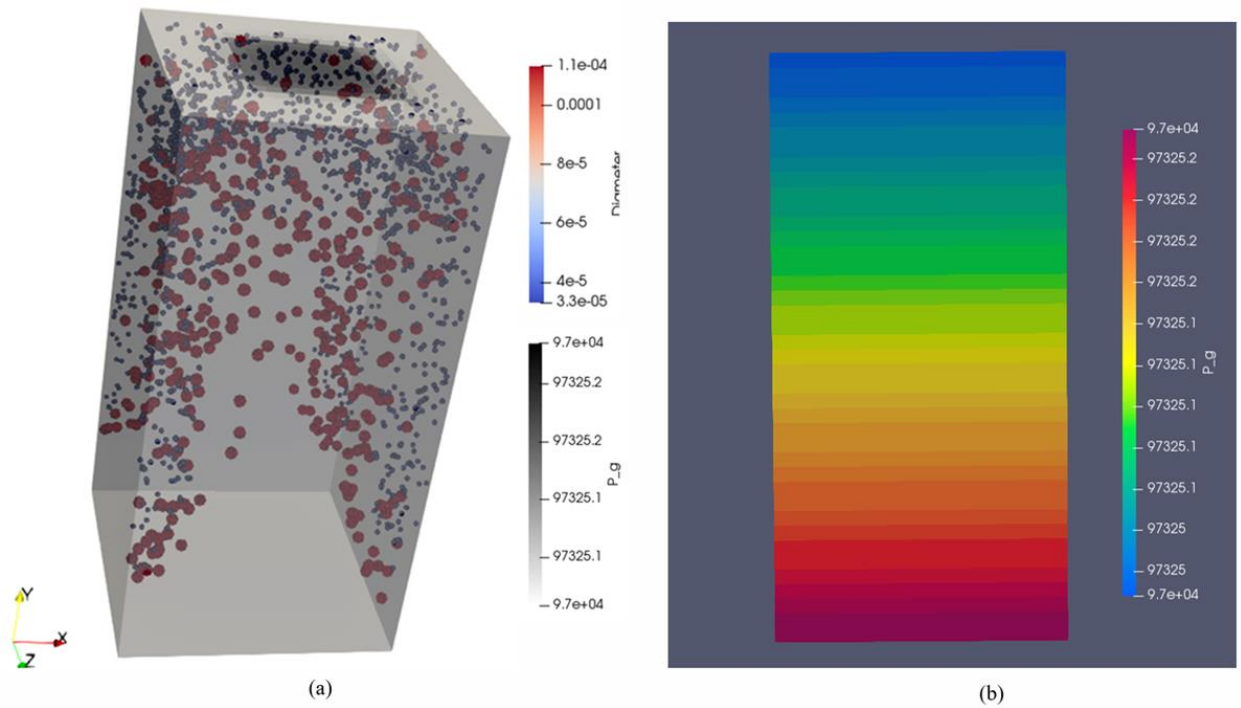

Figure 5.17: Pressure field on MFiX 3D fluidized bed simulation

5.8: Data Analysis for 3D Simulation:

An important parameter for data analysis is determining the key variables as an output parameter using Sampling method. This method creates sets of samples according to the probability distributions of the uncertain variables and sets them into corresponding sets of response functions, where the number of samples is specified by the samples integer specification [117]. Means, standard deviations and 95% confidence intervals are calculated for the response functions.

Table 5.5: Mean and Standard Deviation (SD) values of variables used in the 3D case. All the units are in the SI system.

Variable name	Description of the variable	Mean value	SD
V1	velocity of air	1.5	0.4
V2	viscosity of air	1.8E-05	3.6E-06
V3	drug particle diameter	5.3E-05	1.1E-05
V4	drug particle density	2650	530
V5	carrier particle diameter	3.2E-06	6.4E-07
V6	carrier particle density	1520	304
V7	normal coefficient of restitution for parcel-wall collisions	0.5	0.16
V8	drag correlation	6	2
V9	tangential coefficient of restitution for parcel-wall collisions	0.5	0.166
V10	volume fraction exponential scale factor in frictional stress model	3	0.66
V11	the empirical dampening factor for the frictional stress model,	0.5	0.166
V12	solids slip velocity scale factor	0.5	0.166
V13	density of air	1.205	0.241
V14	the pressure at the top boundary	1atm - 4000	800

Ten different drag models considered in this study are GIDASPOW_BLEND_PCF, BVK, GIDASPOW, GIDASPOW_BLEND, GIDASPOW_PCF, SYAM_OBRIEN, WEN_YU, WEN_YU_PCF, KOCH_HILL, and KOCH_HILL_PCF. Correlation coefficients are important to determine which variables play most vital rules in calculations and show the strength of effects of each parameters. Therefore, instead of focusing on lots of variables it'll be easy to determine the most effective parameter that can dominate the simulation. Correlations are calculated between two sets of sample data. So, the calculation of correlation coefficients can be done between two input variables, between an input and an output variable or between two output variables. The simple correlation coefficients is defined for two variables x and y as: Corr(x; y)= $\frac{\sum_i (x_i - \bar{x})(y_i - \overline{y})}{\sqrt{\sum_i (x_i - \bar{x})^2 \sum_i (y_i - \bar{y})^2}}$. Correlation coefficient varies from 0 to 1. If the value is close to 0, then the variable is negligible and has less effects on simulations.

Table 5.6: Partial Correlation Matrix between input variables and residence time

Input Variable	Input Correlation coefficient with residence time
V1	-9.91E-01
V2	-8.41E-02
V3	-5.52E-02
V4	2.88E-01
V5	2.77E-01
V6	4.53E-01
V7	1.11E-01
V8	4.32E-01
V9	-5.96E-01
V10	7.20E-01
V11	-4.23E-01
V12	-6.99E-02
V13	-3.17E-01
V14	-1.23E-02

Table 5.6 shows correlation coefficients between input variables and residence time. It is seen from the table that air velocity, carrier particle diameter, density and volume fraction plays most dominant role in this 3D DPI simulation. The values close to 1 have more effects on simulation, while values nearly 0 have negligible effects. Solid slip velocity factor and air viscosity effects has minimal effects on this 3D analysis.

In the present study, the data generated with Dakota-MFiX for 500 samples are used for the data-driven framework and 50 points are used for testing. Deep neural network algorithm is used in TensorFlow to predict the mean quantities of interest. The predicted mean QOIs are forwarded to DAKOTA via the C++ wrapper to get the statistics for residence time. The neural network is consists of two hidden layers and one input as well as the output layer. An adaptive gradient-based optimization method is used to lessen the cost function in the neural network. The predicted values from the algorithm are compared with the actual values for the test dataset. In statistics, the actual value is obtained by measuring the available data and the predicted value is the value of the variable predicted based on the regression analysis.

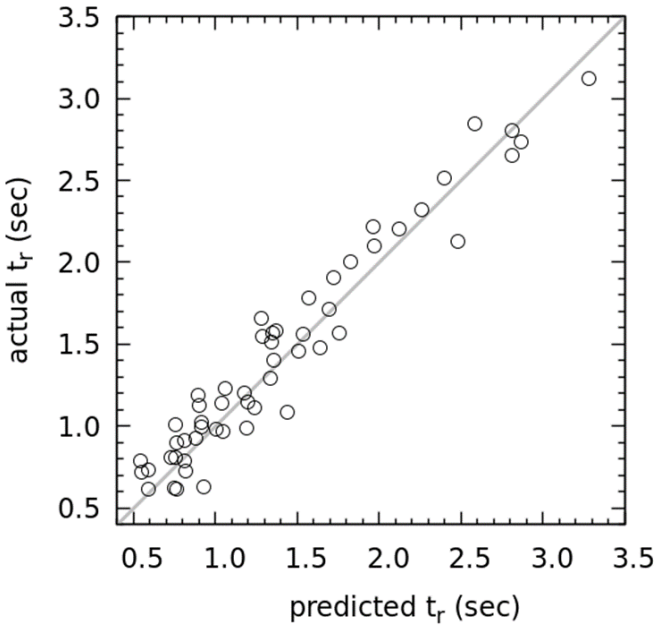

Figure 5.18: Comparison of actual residence time and predicted residence time for 50 cases

Figure 5.18 shows the cumulative probability for the mean quantities of interest in terms of residence time. The predicted residence time from the algorithm for the test dataset are compared with the actual values. Residuals are graphically symbolized by means of a residual plot. When the difference between these values are positive, then the data points are above the regression line and if the difference is negative then the data points are below the regression line. Difference between the actual value and the predicted value is called residual. The residuals play an important role to validate the regression model. On above figure, few of the points are near regression line indicate positive residual values. Most data points lie on the regression line indicates that the difference is zero. As most of the predicted values are close to the actual values in the plot that means it follows linear regression and have a good fit. Most of the predicted values are the same as the computed values over the range of 1-1.65 on Figure 5.18 means that the model can provide an adequate fit and does not need to revise. The mean square and variance for the predicted and actual values are 0.02 and 0.94, respectively.

Usually, uncertainty quantification (UQ) is used to advance the understanding of how variations in the parameters affect the response functions of any computational applications. In this project, UQ is performed by calculating approximate response function distribution statistics based on specified input random variable probability distributions [118]. These response statistics contain response mean, response standard deviation, skewness and kurtosis values. In this study, the data generated with Dakota-MFiX for the sample size of 500 is used for the data-driven framework. The mean and standard deviation of the response function is 1.5386 and 0.533868 respectively.

A deep neural network algorithm is used in the TensorFlow library to attain reliable statistics of mean quantities of interest. The data collected from Dakota-MFiX simulations is used to train as well as validate the machine learning algorithm. The validated algorithm is used to predict mean quantities of interest. The predicted functions are passed to Dakota via the C++ wrapper to obtain statistics of the residence time across the fluidized bed with LHS method based on 500 samples for 14 uncertain input parameters with various distributions. Sampling method shows sets of samples according to the probability distributions of the uncertain variables and maps them into corresponding sets of response functions, when the number of samples is known [117].

Table 5.7: Low order statistics of QoIs for different sample sizes

Samples	**QoI Mean**	**QoI SD**
1000	1.7152	0.6024
10000	1.6844	0.5802
100000	1.3022	0.5062
200000	1.1252	0.4858

Means, standard deviations and 95% confidence intervals are computed for the response functions. Based on 95% confidence intervals for response function, the LowerCI_Mean, UpperCI_Mean, LowerCI_StdDev and UpperCI_StdDev are 1.4917280142e+00, 1.5855450360e+00, 5.0270266567e-01 and 5.6918428097e-01 respectively. With 95% confidence the actual value of each parameter falls between the intervals specified and assume the misfit between the model and corresponding data. The effect of sample size on the QoIs has been studied in this project. The mean value decreases with an increase in the sample size. A similar trend in standard deviation is visible on Table 5.7. It is observed that approximately 100000 samples provide reliable intervals for the QoIs.

5.9: Summary

This study shows the development of a novel high fidelity CFD-DEM method and sensitivity analysis for predicting the transport and deposition of for DPI carrier and API particles with agglomeration and deagglomeration. Current work shows the range of validity for using simulations based on a 2D Cartesian coordinate system to assess a rectangular fluidized bed with different parameter. The simulations has been conducted for different inlet gas velocities with different particle diameter, which correspond to the bubbling and slugging regimes of fluidized beds. Current analysis shows that drug particles of 1-3.66 μm show a higher drug dispersion and better aerosolization behavior with carrier particles between 51-63 μm on basis of residence time. A 3D simulation has been done for large amount of particles using MFiX-PIC model to acquire actual DPI performances. In this study, the data generated with Dakota-MFiX for the sample size of 500 is used for the data-driven framework. The mean and standard deviation of the response function is 1.5386 and 0.533868 respectively. Means, standard deviations and 95% confidence intervals are computed for the response functions. Based on 95% confidence intervals for response function, the LowerCI_Mean, UpperCI_Mean, LowerCI_StdDev and UpperCI_StdDev are 1.4917280142e+00, 1.5855450360e+00, 5.0270266567e-01 and 5.6918428097e-01 respectively.

Chapter 6: Conclusion and Future Works

6.1: Project Summary: Recently besides asthma and COPD, other pulmonary diseases such as cystic fibrosis, lung cancer and pulmonary infectious diseases and also systemic disorders such as diabetes, cancer, neurobiological disorders are considered to be treated by pulmonary drug delivery [78]. Due to DPI's numerous advantages over other pulmonary drug delivery systems, the inhalation performances are trying to be improved by changing, drug and carrier particle engineering and formulation strategy. This research has provided the understanding of aerosol particle behavior within DPI device by identifying the mechanisms and the factors that have the most influence on inhaler behavior. It has shown that this behavior can be portrayed computationally using a CFD-DEM technique and can use DEM a viable tool in the design and virtual testing of new DPI designs. The main objective in this research is to obtain reproducible, high pulmonary deposition by successful particle selection and careful process optimization.

This study shows the development of a novel high fidelity CFD-DEM method and sensitivity analysis for predicting the transport and deposition of for DPI carrier and API particles with agglomeration and deagglomeration [119-121]. Since DPI particle transport is affected by particle-particle interactions, heterogeneous particles sizes and shapes, electrostatic and Van der Waals forces, they show considerable challenges to CFD modelers to model regional lung deposition from a DPI. The combination of computational modeling and sensitivity analysis was used magnificently to validate the models with available data from the literature for DPI for various formulation properties and their effects on particle size distribution with DAKOTA. The uncertainty quantification results with MFiX-DAKOTA framework for the fluidized bed with central jet having uncertain input variables. The average bed height decreases with the decrease in

standard deviation of the input variables that shows good agreement with the results from previous work done with MFiX-PSUADE framework.

For attaining the objectives of the project, this present work shows the range of validity for using simulations based on a 2D Cartesian coordinate system to assess a rectangular fluidized bed with different parameter. The simulations has been conducted for different inlet gas velocities with different particle diameter, which correspond to the bubbling and slugging regimes of fluidized beds. After all these analyses, a novel high fidelity discrete element (CFD-DEM) method and sensitivity analysis is developed for predicting the transport and deposition of carrier and API particles. Ideal particle size is determined based on residence time for better DPI performances and respiratory deposition. Current analysis shows that drug particles of 1-3.66 μm show a higher drug dispersion and better aerosolization behavior with carrier particles between 51-63 μm on basis of residence time. ANSYS FLUENT simulation shows the visualization of fluid and particle flow inside inhaler domain. To acquire real-world DPI performances, a 3D simulation has been done for large amount of particles using MFiX-PIC model which needs to be developed for further analysis. Table 6.1 shows the parameters obtained from present CFD-DEM analysis that can be used for scrutinizing DPI devices performances.

Table 6.1: Anticipated parameter for better DPI performances (based on CFD-DEM method)

Parameter	Value	Unit
Drug particle	1-3.7	μm
Carrier particle	51-63	μm
Desired inlet velocity	2.5	m/s
Particle velocity	0.01	m/s
Pressure drop	4000	Pa

For 3D fluidized bed, a deep neural network algorithm is used in the TensorFlow library to attain reliable statistics of mean quantities of interest. The data collected from Dakota-MFiX simulations is used to instruct and validate the machine learning algorithm. The validated

algorithm is used to predict mean quantities of interest. The predicted functions are passed to Dakota via the C++ wrapper to obtain statistics of the residence time across the fluidized bed with sampling method based on 500 samples for 14 uncertain input parameters with various distributions. While four input parameters show more influence, the remaining ten input parameter's influence on mean quantities of interest is negligible. However, these observations are in good agreement with previous works [68].

6.2: Future Work/Recommendations: Advancements in DPI show a substantial development in pulmonary delivery technology. While current research identifies ideal types of particle size distribution, it does not relate these quantitatively to dose fluidization emerging into the lungs. Current work only focuses on inhaler performances based on particle size distribution and based on these particle sizes, particle transport and respiratory deposition has been presumed. But further experimental work is required to quantitatively correlate the exit particle size distribution to the dose fluidization method. Furthermore, the studies described in this work could be the basis of future research regarding the relation between particle size distribution and inhaler performances. The results presented in this research arise new queries about DPI process and a number of methods for further research are listed below:

- Current work focuses the CFD-DEM method of particle distribution inside DPI device. But the transport and deposition of this size ranges into respiratory track after leaving inhaler domain has not been shown computationally, which can be shown for future advancement of this project.
- Detailed UQ analysis for further 3D MFiX fluidized bed modeling can be added as continuation of this research [122].

- Several design modifications needs to be done on modeling the fluidized bed simulations to develop a novel high fidelity discrete element (CFD-DEM) method. For this purpose, the following parameters needs to be investigated:
    - change of fluid property
    - changes of air pressure
    - vary with different inhaler geometry
- For enhancing the effectiveness of pulmonary drug formulations, particle shape, morphology and hygroscopicity will need to develop which have not been discussed in this research. This approach in future work technologies may enable more drugs to be delivered through for treatment of lung diseases or systemic therapy.
- A comparative study between all models will be beneficial to explore the uncertainty quantification.
- Development of a novel high fidelity discrete element (CFD-DEM) method and sensitivity analysis needs to be carried out using DAKOTA for predicting the transport and deposition as well as the agglomeration and deagglomeration for DPI carrier and API particles.
- Current work has demonstrated that DEM is capable of capturing particle detailed information in DPI, but further work is required to illustrate insights into the dose behavior.
- The dose fluidization have not been investigated in this work, but play an important role in the dose behavior. It depends on several factors like relative humidity, powder preparation processes etc. So, further experiments are necessary to quantify such effects and also dose fluidization.

- The therapeutic efficacy of the inhalation therapy has not been investigated in this project. It can be computed by using clinical parameters only and suitable subject for further research.

References

[1] Alderborn, G., and Aulton, M., 2002, "Pharmaceutics: The Science of Dosage Form Design," Pharm. Sci. Dos. form Des.

[2] Frijlink, H. W., and De Boer, A. H., 2004, "Dry Powder Inhalers for Pulmonary Drug Delivery," Expert Opin. Drug Deliv., **1**(1), pp. 67–86.

[3] Islam, N., and Gladki, E., 2008, "Dry Powder Inhalers (DPIs)—a Review of Device Reliability and Innovation," Int. J. Pharm., **360**(1), pp. 1–11.

[4] Newman, S. P., and Busse, W. W., 2002, "Evolution of Dry Powder Inhaler Design, Formulation, and Performance," Respir. Med., **96**(5), pp. 293–304.

[5] Chan, H.-K., 2006, "Dry Powder Aerosol Delivery Systems: Current and Future Research Directions," J. aerosol Med., **19**(1), pp. 21–27.

[6] Chan, H.-K., 2006, "Dry Powder Aerosol Drug Delivery—Opportunities for Colloid and Surface Scientists," Colloids Surfaces A Physicochem. Eng. Asp., **284**, pp. 50–55.

[7] Zhou, Q. T., Tang, P., Leung, S. S. Y., Chan, J. G. Y., and Chan, H.-K., 2014, "Emerging Inhalation Aerosol Devices and Strategies: Where Are We Headed?," Adv. Drug Deliv. Rev., **75**, pp. 3–17.

[8] Stegemann, S., Kopp, S., Borchard, G., Shah, V. P., Senel, S., Dubey, R., Urbanetz, N., Cittero, M., Schoubben, A., and Hippchen, C., 2013, "Developing and Advancing Dry Powder Inhalation towards Enhanced Therapeutics," Eur. J. Pharm. Sci., **48**(1–2), pp. 181–194.

[9] De Boer, A. H., Chan, H. K., and Price, R., 2012, "A Critical View on Lactose-Based Drug Formulation and Device Studies for Dry Powder Inhalation: Which Are Relevant and What Interactions to Expect?," Adv. Drug Deliv. Rev., **64**(3), pp. 257–274.

[10] Zhou, Q. T., and Morton, D. A., 2012, "Drug–lactose Binding Aspects in Adhesive Mixtures: Controlling Performance in Dry Powder Inhaler Formulations by Altering Lactose Carrier Surfaces," Adv. Drug Deliv. Rev., **64**(3), pp. 275–284.

[11] Begat, P., Morton, D. A., Staniforth, J. N., and Price, R., 2004, "The Cohesive-Adhesive Balances in Dry Powder Inhaler Formulations I: Direct Quantification by Atomic Force Microscopy," Pharm. Res., **21**(9), pp. 1591–1597.

[12] Begat, P., Morton, D. A., Staniforth, J. N., and Price, R., 2004, "The Cohesive-Adhesive Balances in Dry Powder Inhaler Formulations II: Influence on Fine Particle Delivery Characteristics," Pharm. Res., **21**(10), pp. 1826–1833.

[13] Kaialy, W., Alhalaweh, A., Velaga, S. P., and Nokhodchi, A., 2011, "Effect of Carrier Particle Shape on Dry Powder Inhaler Performance," Int. J. Pharm., **421**(1), pp. 12–23.

[14] Guenette, E., Barrett, A., Kraus, D., Brody, R., Harding, L., and Magee, G., 2009, "Understanding the Effect of Lactose Particle Size on the Properties of DPI Formulations Using Experimental Design," Int. J. Pharm., **380**(1–2), pp. 80–88.

[15] McKeon, B. J., Zagarola, M. V., and Smits, A. J., 2005, "A New Friction Factor Relationship for Fully Developed Pipe Flow," J. Fluid Mech., **538**, pp. 429–443.

[16] Zanen, P., Go, L. T., and Lammers, J.-W. J., 1994, "The Optimal Particle Size for β-Adrenergic Aerosols in Mild Asthmatics," Int. J. Pharm., **107**(3), pp. 211–217.

[17] Donovan, M. J., Kim, S. H., Raman, V., and Smyth, H. D., 2012, "Dry Powder Inhaler Device Influence on Carrier Particle Performance," J. Pharm. Sci.

[18] Young, P. M., Edge, S., Traini, D., Jones, M. D., Price, R., El-Sabawi, D., Urry, C., and Smith, C., 2005, "The Influence of Dose on the Performance of Dry Powder Inhalation

Systems," Int. J. Pharm., **296**(1–2), pp. 26–33.
[19] Kaialy, W., Ticehurst, M., and Nokhodchi, A., 2012, "Dry Powder Inhalers: Mechanistic Evaluation of Lactose Formulations Containing Salbutamol Sulphate," Int. J. Pharm., **423**(2), pp. 184–194.
[20] Kaialy, W., and Nokhodchi, A., 2012, "Antisolvent Crystallisation Is a Potential Technique to Prepare Engineered Lactose with Promising Aerosolisation Properties: Effect of Saturation Degree," Int. J. Pharm., **437**(1–2), pp. 57–69.
[21] Cline, D., and Dalby, R., 2002, "Predicting the Quality of Powders for Inhalation from Surface Energy and Area," Pharm. Res., **19**(9), pp. 1274–1277.
[22] Steckel, H., and Bolzen, N., 2004, "Alternative Sugars as Potential Carriers for Dry Powder Inhalations," Int. J. Pharm., **270**(1–2), pp. 297–306.
[23] Jashnani, R. N., Byron, P. R., and Dalby, R. N., 1995, "Testing of Dry Powder Aerosol Formulations in Different Environmental Conditions," Int. J. Pharm., **113**(1), pp. 123–130.
[24] Shur, J., Kubavat, H. A., Ruecroft, G., Hipkiss, D., and Price, R., 2012, "Influence of Crystal Form of Ipratropium Bromide on Micronisation and Aerosolisation Behaviour in Dry Powder Inhaler Formulations," J. Pharm. Pharmacol., **64**(9), pp. 1326–1336.
[25] Adi, H., Kwok, P. C. L., Crapper, J., Young, P. M., Traini, D., and Chan, H.-K., 2010, "Does Electrostatic Charge Affect Powder Aerosolisation?," J. Pharm. Sci., **99**(5), pp. 2455–2461.
[26] Rabbani, N. R., and Seville, P. C., 2005, "The Influence of Formulation Components on the Aerosolisation Properties of Spray-Dried Powders," J. Control. release, **110**(1), pp. 130–140.
[27] Kaialy, W., and Nokhodchi, A., 2013, "Engineered Mannitol Ternary Additives Improve Dispersion of Lactose–salbutamol Sulphate Dry Powder Inhalations," AAPS J., **15**(3), pp. 728–743.
[28] Kaialy, W., Hussain, T., Alhalaweh, A., and Nokhodchi, A., 2014, "Towards a More Desirable Dry Powder Inhaler Formulation: Large Spray-Dried Mannitol Microspheres Outperform Small Microspheres," Pharm. Res., **31**(1), pp. 60–76.
[29] Ruzycki, C. A., Javaheri, E., and Finlay, W. H., 2013, "The Use of Computational Fluid Dynamics in Inhaler Design," Expert Opin. Drug Deliv., **10**(3), pp. 307–323.
[30] Ferziger, J. H., and Perić, M., 2002, *Computational Methods for Fluid Dynamics*.
[31] Wesseling, P., 2001, *Principles of Computational Fluid Dynamics*.
[32] Tu, J., 2012, *Computational Fluid Dynamics A Practical Approach*.
[33] Versteeg, H. K., and Malalasekera, W., 2007, *An Introduction to Computational Fluid Dynamics: The Finite Volume Method*, Pearson Education.
[34] Moskal, A., and Sosnowski, T. R., 2012, "Computational Fluid Dynamics (CFD) and Direct Visualization Studies of Aerosol Release from Two Cyclohaler-Type Dry Powder Inhalers," J. Drug Deliv. Sci. Technol.
[35] Milenkovic, J., Alexopoulos, A. H., and Kiparissides, C., 2013, "Flow and Particle Deposition in the Turbuhaler: A CFD Simulation," Int. J. Pharm.
[36] Milenkovic, J., Alexopoulos, A. H., and Kiparissides, C., 2014, "Deposition and Fine Particle Production during Dynamic Flow in a Dry Powder Inhaler: A CFD Approach," Int. J. Pharm.
[37] Cundall, P. A., and Strack, O. D. L., 1979, "A Discrete Numerical Model for Granular Assemblies," Géotechnique.
[38] Zhu, H. P., Zhou, Z. Y., Yang, R. Y., and Yu, A. B., 2007, "Discrete Particle Simulation of Particulate Systems: Theoretical Developments," Chem. Eng. Sci.

[39] Zhu, H. P., Zhou, Z. Y., Yang, R. Y., and Yu, A. B., 2008, "Discrete Particle Simulation of Particulate Systems: A Review of Major Applications and Findings," Chem. Eng. Sci.
[40] Wong, W., Fletcher, D. F., Traini, D., Chan, H. K., and Young, P. M., 2012, "The Use of Computational Approaches in Inhaler Development," Adv. Drug Deliv. Rev.
[41] Kafui, K. D., Thornton, C., and Adams, M. J., 2002, "Discrete Particle-Continuum Fluid Modelling of Gas-Solid Fluidised Beds," Chem. Eng. Sci.
[42] Xu, B. H., and Yu, a. B., 1997, "Numerical Simulation of the Gas-Solid Flow in a Fluidized Bed by Combining Discrete Particle Method with Computational Fluid Dynamics," Chem. Eng. Sci.
[43] Pei, C., Wu, C. Y., England, D., Byard, S., Berchtold, H., and Adams, M., 2013, "Numerical Analysis of Contact Electrification Using DEM-CFD," Powder Technol.
[44] *P.J. Atkins, T.M. Crowder, The design and development of inhalation drug delivery system. In A.J. Hickey (Ed.), Pharmaceutical Inhalation Aerosol Technology (2nd Ed., pp. 279-310); New York: Marcel Dekker, Inc.*
[45] Noakes T. Medical aerosol propellants. J Fluorine Chem 2002; 118(1– 2):35–45.
[46] Ferguson, G. T., Hickey, A. J., & Dwivedi, S. (2018). Co-suspension delivery technology in pressurized metered-dose inhalers for multi-drug dosing in the treatment of respiratory diseases. Respiratory medicine, 134, 16-23. Davim, J. P. (Ed.). (2013). Biomaterials and medical tribology: research and development. Elsevier.
[47] Juntunen-Backman, K., Kajosaari, M., Laurikainen, K., Malinen, A., Kaila, M., Mustala, L., & Toivanen, P. (2002). Comparison of Easyhaler® metered-dose, dry powder inhaler and a pressurised metered-dose inhaler plus spacer in the treatment of asthma in children. *Clinical drug investigation*, *22*(12), 827-835.
[48] Dolovich, M. B., & Dhand, R. (2011). Aerosol drug delivery: developments in device design and clinical use. *The Lancet*, *377*(9770), 1032-1045.
[49] H.K. Chan, N.Y.K. Chew, Novel alternative methods for the delivery of drugs for the treatment of asthma. Advanced Drug Delivery Reviews, 2003; 55: 793-805.
[50] A.R. Clark, Pulmonary delivery technology: recent advances and potential for the new millennium. In A.J. Hickey (Ed.), Pharmaceutical Inhalation Aerosol Technology (2nd Ed., pp. 571-592); New York: Marcel Dekker, Inc.
[51] Khan, I., Elhissi, A., Shah, M., Alhnan, M. A., & Ahmed, W. (2013). Liposome-based carrier systems and devices used for pulmonary drug delivery. In Biomaterials and Medical Tribology (pp. 395-443). Woodhead Publishing.
[51] Partridge, M. R. (1994). Metered-dose inhalers and CFCs: what respiratory physicians need to know? Respiratory medicine, 88(9), 645-647.
[52] Dalby, R., & Suman, J. (2003). Inhalation therapy: technological milestones in asthma treatment. Advanced drug delivery reviews, 55(7), 779-791.
[53] Chan, H. K. (2006). Dry powder aerosol delivery systems: current and future research directions. Journal of aerosol medicine, 19(1), 21-27.
[54] Leach, C. L. (2005). The CFC to HFA transition and its impact on pulmonary drug development. Respiratory care, 50(9), 1201-1208.
[55] Islam, N., & Cleary, M. J. (2012). Developing an efficient and reliable dry powder inhaler for pulmonary drug delivery–a review for multidisciplinary researchers. Medical engineering & physics, 34(4), 409-427.
[56] Peart, J., & Clarke, M. J. (2001). New developments in dry powder inhaler technology. American Pharmaceutical Review, 4, 37-46.

[57] Voss, A., & Finlay, W. H. (2002). Deagglomeration of dry powder pharmaceutical aerosols. International journal of pharmaceutics, 248(1-2), 39-50.
[58] De Boer, A. H., Hagedoorn, P., Gjaltema, D., Lambregts, D., Irngartinger, M., & Frijlink, H. W. (2004). The rate of drug particle detachment from carrier crystals in an air classifier-based inhaler. Pharmaceutical research, 21(12), 2158-2166.
[59] Calvert, G., Hassanpour, A., & Ghadiri, M. (2011). Mechanistic analysis and computer simulation of the aerodynamic dispersion of loose aggregates. Chemical Engineering Research and Design, 89(5), 519-525.
[60] Frijlink, H. W., & de Boer, A. H. (2005). Trends in the technology-driven development of new inhalation devices. *Drug Discovery Today: Technologies*, *2*(1), 47-57.
[61] Pei, C., Wu, C. Y., Adams, M., England, D., Byard, S., and Berchtold, H., 2015, "Contact Electrification and Charge Distribution on Elongated Particles in a Vibrating Container," Chem. Eng. Sci.
[62] Syamlal, M., Rogers, W., and O'Brien, T. J., 1993, "MFIX Documentation: Theory Guide," Natl. Energy Technol. Lab. Dep. Energy, Tech. Note DOE/METC-95/1013 NTIS/DE95000031.
[63] Syamlal, M., and others, 1998, "MFIX Documentation: Numerical Technique," Natl. Energy Technol. Lab. Dep. Energy, Tech. Note No. DOE/MC31346-5824.
[64] Benyahia, S., Syamlal, M., and O'Brien, T. J., 2006, "Extension of Hill–Koch–Ladd Drag Correlation over All Ranges of Reynolds Number and Solids Volume Fraction," Powder Technol., **162**(2), pp. 166–174.
[65] Strack, O. D. L., and Cundall, P. A., 1978, *The Distinct Element Method as a Tool for Research in Granular Media*, Department of Civil and Mineral Engineering, University of Minnesota.
[66] Garg, R., Galvin, G., Li, T., and Pannala, S., 2015, "Documentation of Open-Source MFIX-DEM Software for Gas-Solids Flows, 2012," Google Sch.
[67] Trucano, T. G., Swiler, L. P., Igusa, T., Oberkampf, W. L., and Pilch, M., 2006, "DAKOTA, A Multilevel Parallel Object-Oriented Framework for Design Optimization, Parameter Estimation, Uncertainty Quantification, and Sensitivity Analysis," Reliab. Eng. Syst. Saf., **91**(10–11), pp. 1331–1357.
[68] Kotteda, V. M. K., Kumar, V., and Spotz, W., 2018, "DAKOTA Integrated with MFiX for UQ Analysis: Sensitivity of Particle Size on Pressure in a Fluidized Bed DEM Simulations," *2018 Workshop on Multiphase Flow Science*, National Energy Technology Laboratory.
[69] Smaldone, G., Cruz-Rivera, M., and Nikander, K., 1998, "In Vitro Determination of Inhaled Mass and Particle Distribution for Budesonide Nebulizing Suspension," J. Aerosol Med., **11**(2), pp. 113–125.
[70] Telko, M. J., and Hickey, A. J., 2005, "Dry Powder Inhaler Formulation," Respir. Care, **50**(9), pp. 1209–1227.
[71] Gel, A., Garg, R., Tong, C., Shahnam, M., and Guenther, C., 2013, "Applying Uncertainty Quantification to Multiphase Flow Computational Fluid Dynamics," Powder Technol., **242**, pp. 27–39.
[72] Peng, T., Lin, S., Niu, B., Wang, X., Huang, Y., Zhang, X., Li, G., Pan, X., and Wu, C., 2016, "Influence of Physical Properties of Carrier on the Performance of Dry Powder Inhalers," Acta Pharm. Sin. B.
[73] Tian, G., Hindle, M., Lee, S., and Longest, P. W., 2015, "Validating CFD Predictions of Pharmaceutical Aerosol Deposition with in Vivo Data," Pharm. Res.

[74] Su, G., and Pidaparti, R. M., 2011, "Generating Nanoparticles for Respiratory Drug Delivery," J. Nanotechnol. Eng. Med.
[75] Kotteda, V. K., Stephens, J. A., Spotz, W., Kumar, V., & Kommu, A. (2019). Uncertainty quantification of fluidized beds using a data-driven framework. *Powder Technology*.
[76] Ladeinde F, Nearon MD. CFD applications in the HVAC&R industry. ASHRAE journal. 1997; 39:44-8.
[77] Hirsch C. Numerical Computation of Internal and External Flows: The Fundamentals of Computational Fluid Dynamics: The Fundamentals of Computational Fluid Dynamics: Butterworth-Heinemann; 2007.
[78] Bernardo S, Mori M, Peres A, Dionísio R. 3-D computational fluid dynamics for gas and gas-particle flows in a cyclone with different inlet section angles. Powder Technology. 2006; 162(3):190-200.
[79] Chu K, Wang B, Xu D, Chen Y, Yu A. CFD–DEM simulation of the gas–solid flow in a cyclone separator. Chemical Engineering Science. 2011;66(5):834-47.
[80] Chu K, Yu A. Numerical simulation of complex particle–fluid flows. Powder Technology. 2008;179(3):104-14.
[81] Tsuji Y, Tanaka T, Ishida T. Lagrangian numerical simulation of plug flow of cohesionless particles in a horizontal pipe. Powder technology. 1992;71(3):239-50.
[82] Xu B, Yu A. Numerical simulation of the gas-solid flow in a fluidized bed by combining discrete particle method with computational fluid dynamics. Chemical Engineering Science. 1997;52(16):2785-809.
[83] Li Y, Zhang J, Fan L-S. Numerical simulation of gas–liquid–solid fluidization systems using a combined CFD-VOF-DPM method: bubble wake behavior. Chemical Engineering Science. 1999;54(21):5101-7.
[84] Rhodes M, Wang X, Nguyen M, Stewart P, Liffman K. Use of discrete element method simulation in studying fluidization characteristics: influence of interparticle force. Chemical Engineering Science. 2001;56(1):69-76.
[85] Kafui K, Thornton C, Adams M. Discrete particle-continuum fluid modelling of gas–solid fluidised beds. Chemical Engineering Science. 2002;57(13):2395-410.
[87] Yu AB, Xu BH. Particle-scale modelling of gas–solid flow in fluidisation. Journal of Chemical Technology and Biotechnology. 2003;78(2-3):111-21.
[88] Limtrakul S, Boonsrirat A, Vatanatham T. DEM modeling and simulation of a catalytic gas–solid fluidized bed reactor: a spouted bed as a case study. Chemical Engineering Science. 2004;59(22):5225-31.
[89] Di Renzo A, Di Maio FP. Homogeneous and bubbling fluidization regimes in DEM–CFD simulations: hydrodynamic stability of gas and liquid fluidized beds. Chemical Engineering Science. 2007;62(1):116-30.
[90] Tsuji Y. Multi-scale modeling of dense phase gas–particle flow. Chemical Engineering Science. 2007;62(13):3410-8.
[91] Malone K, Xu B. Particle-scale simulation of heat transfer in liquid-fluidised beds. Powder Technology. 2008;184(2):189-204.
[92] Kawaguchi T, Tanaka T, Tsuji Y. Numerical simulation of two-dimensional fluidized beds using the discrete element method (comparison between the two-and three-dimensional models). Powder technology. 1998;96(2):129-38.

[93] Ibsen CH, Helland E, Hjertager BH, Solberg T, Tadrist L, Occelli R. Comparison of multifluid and discrete particle modelling in numerical predictions of gas particle flow in circulating fluidised beds. Powder Technology. 2004;149(1):29-41.
[94] Tryggvason G, Bunner B, Esmaeeli A, Juric D, Al-Rawahi N, Tauber W, et al. A front-tracking method for the computations of multiphase flow. Journal of Computational Physics. 2001;169(2):708-59.
[95] Chu K, Wang B, Yu A, Vince A, Barnett G, Barnett P. CFD–DEM study of the effect of particle density distribution on the multiphase flow and performance of dense medium cyclone. Minerals Engineering. 2009;22(11):893-909.
[96] Chu K, Wang B, Yu A, Vince A. CFD-DEM modelling of multiphase flow in dense medium cyclones. Powder Technology. 2009;193(3):235-47.
[97] Liu D, Bu C, Chen X. Development and test of CFD–DEM model for complex geometry: A coupling algorithm for Fluent and DEM. Computers & Chemical Engineering. 2013;58:260-8.
[98] Batchelor GK. An introduction to fluid dynamics: Cambridge university press; 2000.
[99] Peyret R, Taylor TD. Computational methods for fluid flow. New York, Springer-Verlag, 1985, 368 p. 1985;1.
[100] Elsayed K, Lacor C. A CFD Study of the Effects of Cone Dimensions on the Flow Field of Cyclone Separators using LES.
[101] Boysan F, Ayers W, Swithenbank J. A fundamental mathematical modelling approach to cyclone design. Transactions of the Institution of Chemical Engineers. 1982;60(4):222-30.
[102] Hoffmann AC, Stein LE. Gas Cyclones and Swirl Tubes: Principles, Design, and Operation: Springer; 2007.
[103] Fluent-Inc. "Fluent 6.3. User's Guide,". Fluent Inc; 2006.
[104] Krist SL, Biedron RT, Rumsey CL. CFL3D user's manual (version 5.0): Citeseer; 1998.
[105] Crowe CT, Schwarzkopf JD, Sommerfeld M, Tsuji Y. Multiphase flows with droplets and particles: CRC press; 2011.
[106] Abadi, M., Agarwal, A., Barham, P., Brevdo, E., Chen, Z., Citro, C., ... & Ghemawat, S. (2016). Tensorflow: Large-scale machine learning on heterogeneous distributed systems. *arXiv preprint arXiv:1603.04467*.
[107] Wongsuphasawat, K., Smilkov, D., Wexler, J., Wilson, J., Mane, D., Fritz, D., ... & Wattenberg, M. (2017). Visualizing dataflow graphs of deep learning models in tensorflow. *IEEE transactions on visualization and computer graphics*, *24*(1), 1-12.
[108] Meyer, T., Schulz, H., Brand, P., Kohlhäufl, M., Heyder, J., & Häussinger, K. (2001). Totraumbestimmung nach Fowler bei Patienten mit Lungenemphysem mit Hilfe von C18O2. *Pneumologie*, *55*(03), 126-129.
[109] Quanjer, P. H., Tammeling, G. J., Cotes, J. E., Pedersen, O. F., Peslin, R., & Yernault, J. C. (1993). Lung volumes and forced ventilatory flows.
[110] Hamishehkar, H., Rahimpour, Y., & Javadzadeh, Y. (2012). *The role of carrier in dry powder inhaler* (Vol. 3). chapter.
[111] C. N. Davies. Definitive equations for the fluid resistance ofspheres. *Pro. Phys. Soc.* **57**:259–270 (1945).
[112] P. C. Reist. *Aerosol Science and Technology*. McGraw-Hill, New York, 1993.
[113] W. C. Hinds. *Aerosol Technology: Properties, behavior and measurement of airborne particles*. Wiley, New York, 1999.

[114] https://aerosol.ees.ufl.edu/aerosol_trans/section07.html.
[115] Allen, T. (2013). *Particle size measurement*. Springer.
[116] Heyder, J. J. G. C. F. W., Gebhart, J., Rudolf, G., Schiller, C. F., & Stahlhofen, W. (1986). Deposition of particles in the human respiratory tract in the size range 0.005–15 μm. *Journal of aerosol science*, *17*(5), 811-825.
[117] Adams, B. M., Bohnhoff, W. J., Dalbey, K. R., Eddy, J. P., Eldred, M. S., Gay, D. M., ... & Swiler, L. P. (2009). DAKOTA, a multilevel parallel object-oriented framework for design optimization, parameter estimation, uncertainty quantification, and sensitivity analysis: version 5.0 user's manual. *Sandia National Laboratories, Tech. Rep. SAND2010-2183*.
[118] Eldred, M. S., Agarwal, H., Perez, V. M., Wojtkiewicz Jr, S. F., & Renaud, J. E. (2007). Investigation of reliability method formulations in DAKOTA/UQ. *Structure and Infrastructure Engineering*, *3*(3), 199-213.
[119] Antara Badhan, V M Krushnarao Kotteda, Vinod Kumar,2019, CFD DEM Analysis of a Dry powder Inhaler, ASME-JSME-KSME 2019 Joint Fluids Engineering Conference, July 28-August 1, San Francisco, CA
[120] V Kumar, VMK Kotteda, and A Badhan, CFD DEM analysis of a DPI with containerized MFiX on Cloud, National Energy Technology Laboratory's (NETL) 2019 Workshop on Multiphase Flow Science, August 6 -8, 2019, Morgantown, WV, USA. https://mfix.netl.doe.gov/workshop-files/2019/Presentations/NETL_Aug_7/Session_7/05-CFD_DEM_Analysis_of_a_Dry_Powder_Inhaler/CFD_DEM_Analysis_of_a_Dry_Powder_Inhaler.pdf
[121] A Badhan, VMK Kotteda and V Kumar, Numerical analysis of flow in a Dry powder Inhaler, Journal of the Medical Devices (submitted) 2019. https://asmedigitalcollection.asme.org/medicaldevices
[122] A Badhan, VMK Kotteda and V Kumar, Uncertainty quantification of carrier and drug particles residence time in a dry powder Inhaler, ASME Fluids Engineering Summer Conference, July 12 – 16, 2020, Rosen Shingle Creek, Orlando, FL (in preparation) https://event.asme.org/FEDSM

Appendix:

α = Thermal diffusivity [m2/s]

λ = Thermal conductivity [W/m.K]

ρ = Density [kg/m3]

ε = Volume fraction

I_{gm} = Momentum between the fluid phase and the m^{th} solid phase

$\overline{\overline{S}}_g$ = Stress tensor

$\overline{\overline{\tau}}_g$ = Stress tensor

μ_g = Dynamic coefficients of viscosity

λ_g = Second coefficients of viscosity

g = Gravity

Cc = Cunningham slip correlation constant

G = Incident radiation [W/m2]

J = Molecular diffusion flux [mol / (m2-s)]

P = Pressure [Pa]

V = Volumetric flow rate [m3/L]

M = Molecular mass [kg]

Vita

Antara Badhan was born in Dhaka, Bangladesh. He did his B.Sc. in Civil Engineering from the Khulna University of Engineering & Technology (KUET) Khulna, Bangladesh and started her M.S. in the Mechanical Engineering Department at the University of Texas at El Paso in January 2013, where she was a part of cSETR Computational Research Lab under NASA Center for Space Exploration Technology Research at UTEP. After finishing M.S. degree, she started her PhD. in the Environmental Science & Engineering Department at UTEP. While pursuing her degrees she worked as a Research Assistant in the NASA Center for Space Exploration Technology Research (cSETR). She has published her research findings in multiple conference proceedings.

Contact Information: abadhan@miners.utep.edu